4

RESULTS AND DISCUSSION

In the ancient times the people around the world mainly in the Asian countries like India, Japan, China and some African countries used plants for the treatment of various diseases including cancer, fever, oxidative stress mediated diseases, pain, depression, diarrhea, thrombosis and fever. The plants are widely used for treating various diseases because of their low cost and more availability (Jahan and Ahmet, 2020). The plants possess medicinal property due to the presence of various phytochemicals including terpenoids, flavanoids, tannins, polyphenols and lignins (Alam *et al.*, 2021).

In recent times, the nanotechnology is extensively applied in medicine field due to the unique properties of the nanomaterials including chemical, physical and optical properties. Silver nanoparticles are known for their anticancer and antimicrobial potential. Silver nanoparticles carry the anticancer drugs to the tumor site. The cancer cells take up the silver nanoparticles which leads to the death of these cells. So the targeted drug delivery for cancer is possible with the help of silver nanoparticles (Gomes *et al.*, 2021).

Liposomes are lipid vesicles that are used as a carrier for drug delivery to the targeted site. Their major advantage is, they are biodegradable and biocompatible and also they can incorporate both hydrophilic and hydrophobic drugs. They can even encapsulate nanoparticles into them. Liposomes acts as protective vesicle for the drug that is being encapsulated and protect it from any physiological degradation. They usually extend the shelf life of the encapsulated drug and also exhibits controlled release. They exert targeted drug delivery thereby preventing unwanted side effects (Liu *et al.*, 2022).

In tune with the above cited literature, the present study focuses on synthesizing silver nanoparticles loaded liposomes for the targeted therapy of leukaemia. Therefore, an attempt was made to synthesize and characterize silver nanoparticles and silver nanoparticles loaded liposomes, evaluation of drug release profile of the silver nanoparticles loaded liposomes and to analyze the antioxidant and anticancer potential of the various treatment groups.

The present study is divided into four phases and the results are discussed under the following headings.

Phase I

4.1 Synthesis and characterization of silver nanoparticles and silver nanoparticles loaded liposomes of *Tabebuia pallida*

4.1.1. Preliminary Studies

4.1.2. Sunlight mediated green synthesis of silver nanoparticles

4.1.3. Optimisation of plant extract for the synthesis of silver nanoparticles- UV-Vis spectrum analysis

4.1.4. Characterisation of the green synthesized *Tabebuia pallida* silver nanoparticles

4.1.4.1. UV-Vis spectroscopy

4.1.4.2. Elemental mapping

4.1.4.3. X-ray diffraction

4.1.5. Synthesis and Characterization of silver nanoparticles and silver nanoparticles loaded liposomes

4.1.5.1. Encapsulation Efficiency of AgNP loaded Liposomes

4.1.5.2. FTIR Analysis

4.1.5.3. Field Emission Scanning Electron Microscopy

4.1.5.4. Dynamic Light Scattering

4.1.5.5. Zeta Potential

Phase II

4.2 Evaluation of Drug Release profile of AgNPs Loaded Liposomes

4.2.1. *in vitro* Drug Release Profile of AgNPs Loaded Liposomes

4.2.2 Mathematical models used to analyze the efficacy or characteristics of Drug Release

4.2.2.1. Zero Order Model

4.2.2.2. First Order Model

4.2.2.3. Higuchi model

4.2.2.4. Korsmeyer and peppas model

4.2.2.5. Hixson crowel model

Phase III

4.3. Evaluation of Antioxidant Potential of AgNPs and AgNPs Loaded Liposomes

4.3.1. DPPH Radical Scavenging Assay
4.3.2. ABTS Radical Scavenging Assay
4.3.3. Hydroxyl Radical Scavenging Assay
4.3.4. Hydrogen Peroxide Radical Scavenging Assay
4.3.4. Reducing Power Assay
4.3.5. Nitric Oxide Radical Scavenging Assay

Phase IV

4.4. Evaluation of Anticancer potential of AgNPs of *T. pallida* leaves and their Nanoliposomes

4.4.1. MTT Dye Reduction Assay
4.4.2. SRB Assay
4.4.3. Measurement of Apoptosis- Annexin V/FITC staining
4.4.4. Analysis of Mitochondrial Membrane Potential by JC1 Staining
4.4.5. Cell Cycle Analysis

Phase I

4.1. Synthesis and characterization of silver nanoparticles and silver nanoparticles loaded liposomes of *Tabebuia pallida*

4.1.1. Preliminary Studies

Soxhlet extraction of *Tabebuia pallida* leaves were carried out using seven different solvents with decreasing polarity like Water, Methanol, Ethanol, Chloroform, Acetone, Ethyl Acetate, Petroleum Ether and Benzene, and *in vitro* free radical scavenging assays like DPPH radical scavenging assay, ABTS radical scavenging assay, Hydroxyl radical scavenging assay, Hydrogen Peroxide Radical Scavenging Assay, Reducing power assay and Nitric oxide radical scavenging assay were performed for the seven different extracts. Among the tested extracts, the ethanol and water extracts possessed good scavenging potential against all the tested radicals. So an attempt was made to carry out the extraction of phytoconstituents using different proportion of ethanol and water like ethanol 20: water 80, ethanol 80: water 20, ethanol 40:

water 60, ethanol 60: water 40, and ethanol 50: water 50 for synthesizing the silver nanoparticles.

4.1.2. Sunlight mediated green synthesis of silver nanoparticles

Silver nanoparticles synthesis was done using 7 different combinations of various solvents like water, ethanol, ethanol 20: water 80, ethanol 80: water 20, ethanol 40: water 60, ethanol 60: water 40, and ethanol 50: water 50 by mixing with the 1mM aqueous solution of silver nitrate. On exposure to direct sunlight the silver ions were reduced to AgNPs which were confirmed by the colour transformation of the solution from green, the natural colour of the extract to dark reddish brown. (Das *et al.,* 2017). From this colour change, it is clearly evident that *Tabebuia pallida* extracts acts as an effective reducing agent that reduces silver ions to silver nanoparticles.

Before exposure to sunlight

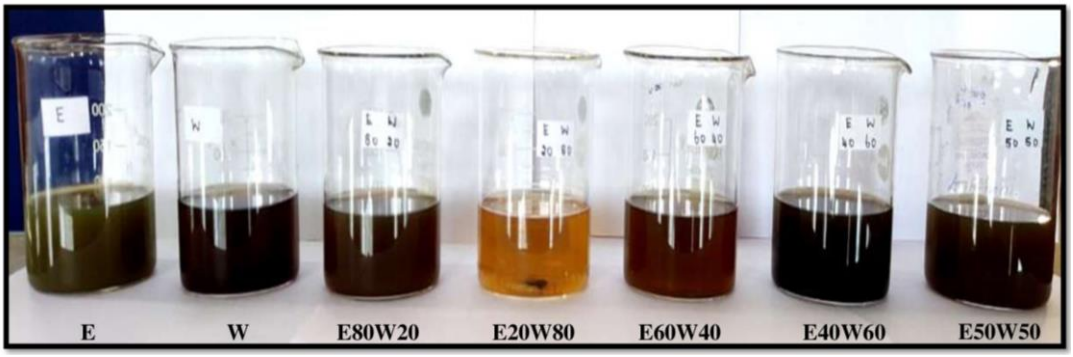

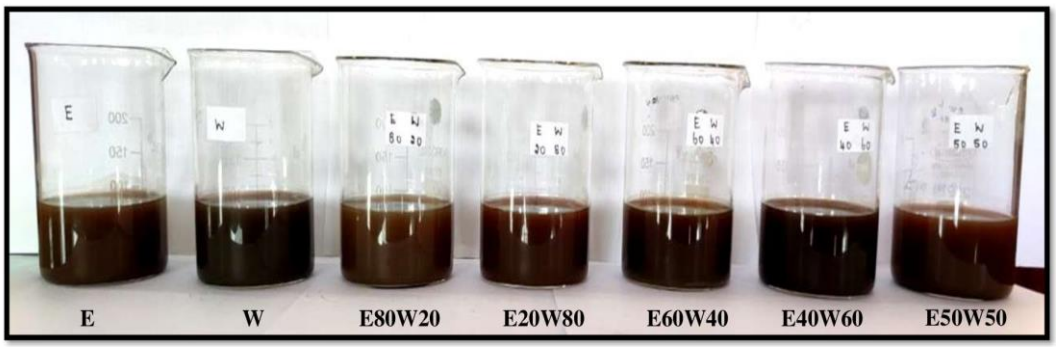

After exposure to sunlight for 30 mins

Fig. 10: Synthesis of silver nanoparticles from various extracts of *Tabebuia pallida*

Vinh *et al.,* (2020) made an attempt to synthesize silver nanoparticles from Pomelo peel extract and observed a colour change from yellow to reddish brown which indicates its reducing ability. Mounil *et al.,* (2020) also reported similar results with *Azadirachta indica* leaf

extract for the synthesis of silver nanoparticles. In line with our study, Fueangfahkan *et al.,* (2020) carried out AgNPs synthesis using Durian rind extract and observed a colour change from pale yellow to dark brown. They reported that this colour change is due to the electron oscillations on the nanoparticles surface, a phenomenon known as surface Plasmon resonance. The synthesis of silver nanoparticles using *Vaccinium arctostaphylos* fruit aqueous extract is noticed by the change in solution colour from pink to dark red (Khodadadi *et al.,* 2021). Vivek *et al.,* (2021) carried out silver nanoparticles synthesis using *Ocimum tenuiflorum* aqueous extract and reported a colour change from light yellow to brownish yellow due to the reduction of silver ions to AgNPs. It is clearly evident that various phytochemicals available in the plant extracts are involved in the reduction process.

In accordance with the above findings *Tabebuia pallida,* the candidate plant of the present study also exhibits the reducing ability which reduces the silver ions to silver nanoparticles which is further confirmed by the color transformation of the solution from green to dark reddish brown. This reducing ability is achieved by the presence of various secondary metabolites present in the plant extracts of various solvents. This colour change is due to the surface Plasmon resonance excitation in the solution.

4.1.3. Optimisation of plant extract for the synthesis of silver nanoparticles by UV-Vis spectral analysis

UV-Vis spectrum analysis is mainly used for confirming whether the synthesized materials are nanoparticles (Mahadevan *et al.,* 2017). UV-Vis spectra of the silver nanoparticles of various compositions of water and ethanol extracts were measured from 200-800 nm (Fig. 3). Usually the silver nanoparticles are found to exhibit absorption maximum in the range of 400-500 nm (Sedighe *et al.,* 2021). UV-Vis spectrum analysis was carried to identify which composition of the extract is suitable for the synthesis of silver nanoparticles. All the compositions showed absorption peaks between 400-500 nm except Ethanol 80: Water 20 which does not show significant absorption peaks. Among the various compositions analysed Ethanol 60: Water 40 was chosen for the further characterisation and analysis since it shows a prominent and little narrowed peak at 450nm where the others showed noise and broadened peaks.

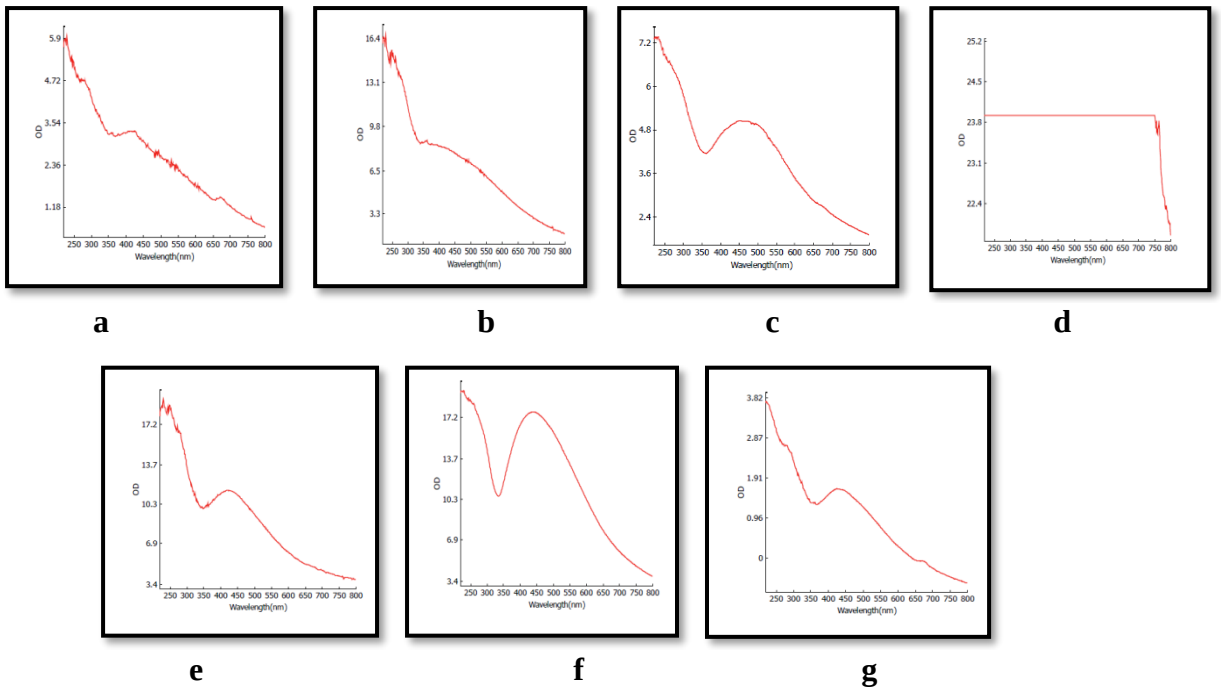

Fig. 11: UV-Vis spectral analysis for the synthesized silver nanoparticles using various proportion of water and ethanol extracts

a-Ethanol; b-Water; c- Ethanol 20:Water 80; d- Ethanol 80:Water 20; e- Ethanol 40:Water 60; f-Ethanol 60:Water 40; g-Ethanol 50:Water 50.

4.1.4. Characterisation of the green synthesized *Tabebuia pallida* silver nanoparticles and silver nanoparticles loaded liposomes

The AgNPs and AgNPs loaded liposomes were characterised using UV-Vis spectroscopy, Fourier transform infrared spectroscopy (FTIR) analysis, Field Emission Scanning Electron Microscope (FESEM), Dynamic Light Scattering (DLS) and X-ray diffraction (XRD).

4.1.4.1. UV-Vis spectroscopy

UV-Vis spectroscopy is a technique that is used to monitor the nanoparticles formation in the initial stages of preparation. When the nanoparticles are synthesized from their corresponding salts it exhibits a strong and well defined peak in the visible region. From the previous studies conducted by many researchers, it is concluded that UV-Vis absorption band between 200-800 nm serves the best for nanoparticles characterization. Usually the conduction bands and valence bands of the silver nanoparticles will be nearer to each other which facilitates the motion of electrons ease that gives rise to a surface Plasmon resonance peak. The absorption

of silver nanoparticles depends on the particle size, dielectric medium and chemicals in the surroundings (Almatroudi and Ahmed, 2020).

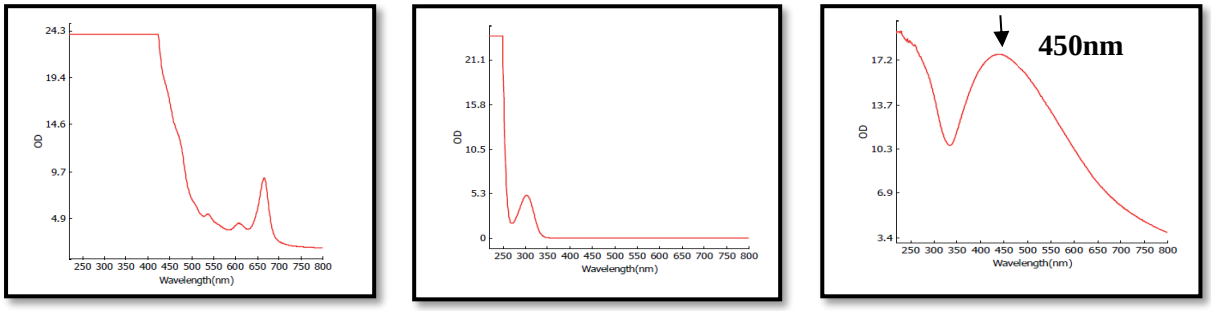

a **b** **c**

a- Hydroethanolic extract; b- Silver nitrate; c- Silver nanoparticle

Fig. 12: UV-Vis spectral analysis of the synthesized silver nanoparticles

The UV-Vis spectra of the hydroethanolic extract of *T. pallida*, silver nitrate and synthesized silver nanoparticles were measured from 200-800nm. The green synthesized *Tabebuia pallida* silver nanoparticles exhibited a strong, well defined, single spectrum at 450 nm which is the characteristics of the AgNPs. According to Mie's theory, single absorption spectra indicate that the silver nanoparticles formed will be spherical in shape. Whereas the particles that are anisotropic in nature exhibits two or more absorption peaks based on their shape (François *et al.*, 2016). In the present study the synthesized AgNPs exhibited a single surface Plasmon resonance band (Fig. 12c) which confirms their spherical shape.

In line with our study, Almasoud *et al.*, (2020) green synthesized silver nanoparticles using *Ficus carica* and *Salvia rosmarinus leaf extracts* and observed a characteristic UV-Vis peak at 450 nm. Sedighe *et al.*, (2021) recorded absorption peak at 443 nm for AgNPs prepared from leaves of *Vaccinium arctostaphylos.* Our results are in par with Dogiparthi *et al.*, (2021) who observed maximum absorption band at 440 nm for the silver nanoparticles synthesized using *Micrargeria wightii* extract. Silver nanoparticles of tomato fruit extract showed a peak at 450 nm (Kishore *et al.*, 2020). Silver nanoparticles synthesized using *Mangifera indica* seed aqueous extract by Savan and Sumitra (2021) exhibited the typical silver Plasmon absorption maxima at 450 nm.

In agreement with the above reports, the results of the present study confirm the formation of spherical shaped silver nanoparticles of *Tabebuia pallida* leaf extract, which is

evident from the single peak at 450 nm in UV-Vis spectroscopy. These synthesized silver nanoparticles were further analyzed for their characterization.

4.1.4.2. Elemental mapping

EDX analysis is employed to assess the relative abundance, composition of elements and purity of the synthesized AgNPs. The X-rays emitted by the silver nanoparticles are detected using EDX technique. The EDX ray detector will quantify the X rays that are discharged based on their energy. The presence of AgNPs can be confirmed by the presence of strong signal peaks at 3 KeV. (Talabani *et al.*, 2021; Bamal *et al.*, 2021)

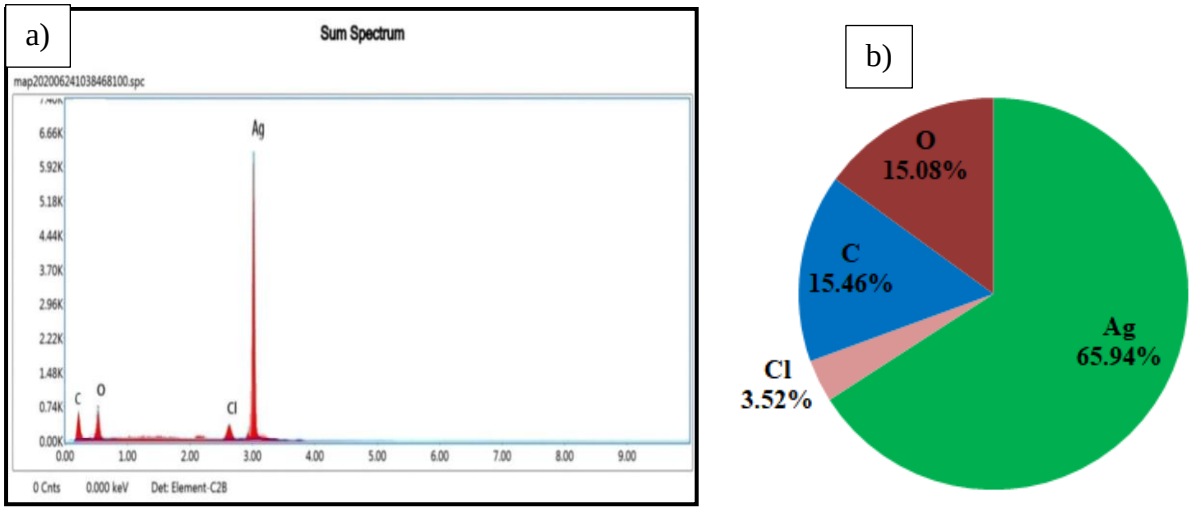

a- Energy dispersive spectrum of silver nanoparticles; b- % weight of various elements in silver nanoparticles.

Fig. 13: Energy dispersive X-ray spectrum of AgNPs synthesized using *Tabebuia pallida*

Fig. 13 shows the EDX spectral analysis of AgNPs synthesized from hydroethanolic extract of *Tabebuia pallida*. An intense EDAX peak at 3 KeV was noticed which is the characteristic of the AgNPs because of their surface Plasmon resonance. From EDAX analysis, it is confirmed that the percentage weight of silver (Ag) was 65.94. Other weak signals with the characteristic absorption of various elements like chlorine (Cl), Oxygen (O) and Carbon (C) was observed with the percentage weight of 3.52, 15.08, 15.46 respectively which may be due to interference of various phytoconstituents available in the plant samples that played acted as reducing agents.

In agreement with our work, Jain and Mehata (2017) synthesized AgNPs using *Ocimum Sanctum* leaf extract, they recorded a sharp peak at 3 KeV for silver nanoparticles and observed

that the percentage weight of silver was 54.87 and the other elements like oxygen, chlorine and carbon were also observed with the percentage weight of 17.25, 4.97 and 22.91 respectively. They reported that the interference of other elements except Ag is due to the secondary metabolites available in the plant samples that are involved in the reduction process. Similar findings were also observed by Karthik *et al.,* (2020), identified an intense signal for Ag at 3 KeV using silver nanoparticles of *Ocimum sanctum* and *Ocimum gratissimum* leaf extracts. The EDAX pattern of the silver nanoparticles from *A. esculentus* flower extract revealed the presence of prominent peak at 3KeV for silver (Devanesan and Alsalhi, 2021). The elemental composition of AgNPs synthesized from *Cucumis prophetarum* leaf extract revealed an intense peak at 3KeV which corresponds to the silver element (Hemlata *et al.,* 2020). The EDAX signal of silver nanoparticles produced by Brassicaceae seeds confirmed the presence of silver which was confirmed by the intense signal at 3 KeV (Rehana *et al.,* 2021).

The present study results are in agreement with the above mentioned literatures which clearly indicate that the predominant element present in the synthesized silver nanoparticles is silver as it constituents 65.94%.

4.1.4.3. X-ray diffraction (XRD):

XRD is a conventional technique that is used in the characterization of silver nanoparticles. It is used in the determination of crystalline structure, size, nature of the phase, of the synthesized AgNPs (Mourdikoudis *et al.,* 2021). The XRD pattern of the prepared silver AgNPs is shown in the Fig. 14. The X ray diffraction pattern of synthesized silver nanoparticles reveals various major diffraction peaks at 21.60°, 27.82°, 32.20°, 38.08°, 46.18°, 54.80°and 57.47° which corresponds the (111), (220), (111), (200), (120), (202), (121) planes respectively (JCPDS 76-1393). These diffraction patterns indicate the existence of FCCC structure of the synthesized nanoparticles. The high intensity of these diffraction peaks indicates the crystalline nature of the AgNPs. Using the 2θ values of the diffraction pattern, the particle size was calculated using Scherrer equation. The size of silver nanoparticles was 10.52 nm at 2θ=21.6039°, 51.12 nm at 2θ=27.8273°, 46.96 nm at 2θ=32.2066°, 21.87 nm at 2θ=38.0854°, 38.53 nm at 2θ=46.1882°, 27.95 nm at 2θ= 54.8036° and 28.29 nm at 2θ=57.4705° (XRD Crystallite (grain) Size Calculator (Scherrer Equation) – InstaNANO, 2022). The mean size was found to be 32.18 nm which is almost similar to the average size obtained using FE-SEM analysis.

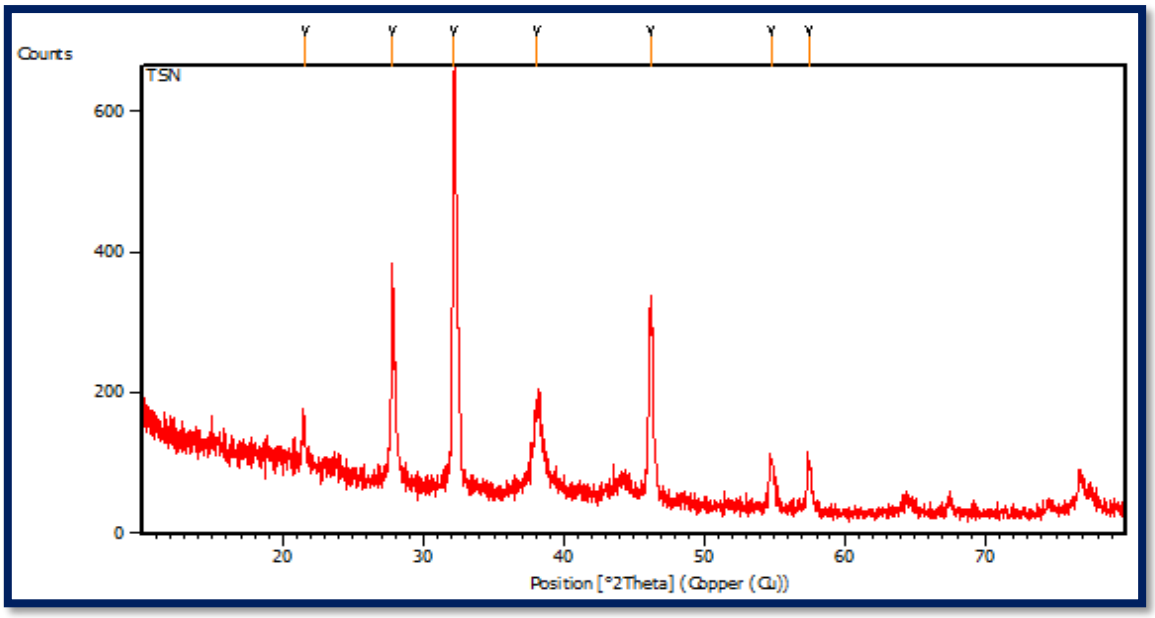

Fig. 14: X-ray diffraction spectrum of AgNPs synthesized using *Tabebuia pallida*

Table 2: X-ray diffraction of AgNPs synthesized using *Tabebuia pallida*

S.No	Pos. [°2Th.]	Height [cts]
1	21.6039	33.36
2	27.8273	300.69
3	32.2066	580.30
4	38.0854	124.06
5	46.1882	262.71
6	54.8036	67.08
7	57.4705	68.09

The XRD spectrum of the prepared AgNPs using *Plantago lanceolata* extract showed different diffraction peaks at 2θ values 23.52°, 27.83°, 38.23°, 44.25°, 46.23°, 54.80°and 57.50°. The intensity of these peaks is very high which confirms the crystalline nature of the synthesized AgNPs. From the nature of these peaks it is elucidated that the synthesized AgNPs are FCCC in structure. The size of the synthesized silver nanoparticles was found to be 30±4 nm (Shah *et al.*, 2021). Similar results were obtained by (Hemlata *et al.*, 2020) who synthesized

AgNPs Using *Cucumis prophetarum* extract and subjected to characterization using XRD analysis. From the XRD analysis, it is confirmed that the synthesized AgNPs are FCCC in nature with diffraction pattern at 2θ values 32.18°, 38.04°, 46.13°, 54.63°, and 77.08° which corresponds to the (111), (200), (120), (202), and (311) planes, respectively. The X- Ray diffraction pattern of the *A. esculentus (L.)* pulp extract showed sharp 2θ peaks at 27.2°, 31.63°, 45.66°, 54.24°, and 57.04° which indicates the FCCC nature of the nanoparticles (Masud *et al.,* 2020). The various peaks at 2θ values 27.82°, 38.08° coincides with the XRD pattern of the green synthesized AgNPs using *Salvia officinalis* aqueous leaf extract which indicates the FCCC structure of the nanoparticles (Okaiyeto *et al.,* 2021).

Thus, it can be concluded that the green synthesized *Tabebuia pallida* silver nanoparticles are FCCC in structure with the mean size of about 32.18 nm. The nanoparticles size has a great influence on the X ray diffraction pattern. The various phytoconstituents present in the plant extracts played a role as capping agent and stabilized the silver nanoparticles which results in the crystalline nature of the AgNPs (Rasheed *et al.,* 2018). Thus from the results obtained, it can be inferred that the green synthesized *Tabebuia pallida* leaf extracts resulted in a spherical nanoparticle formation comprises 68.95% of silver with face centered cubic crystalline nature. Since the *Tabebuia pallida* leaf extracts could render a good support for nanoparticle synthesis. It becomes imperative to prepare a liposome carrier for the synthesized nanoparticles to achieve targeted delivery of the plant extract.

4.1.5. Synthesis of silver nanoparticles loaded liposomes

The AgNPs loaded liposomes were prepared using thin film hydration method coupled with sonication using triglyceride lipid lecithin and cholesterol in the molar ratio 2:1. Chloroform was used as the dissolving solvent for lipids. Thus formed liposomes were characterized using FESEM analysis, Dynamic light Scattering, FTIR analysis and Zeta potential analysis.

4.1.5.1. Encapsulation efficiency

The amount of drug that is encapsulated into a drug delivery system is very much important since it has its direct role in the therapeutic effect of the system. Encapsulation efficiency is defined as the percentage of drug or nanoparticles that is entrapped successfully by the lipid vesicle. Encapsulation efficiency will be affected by many factors including

incubation time, composition of lipid, lipid to drug ratio and pH of the aqueous phase. The encapsulation efficiency is calculated using the formula

$$\text{Encapsulation Efficiency} = \frac{\text{Amount of Encapsulated Nanoparticle}}{\text{Amount of Encapsulated } + \text{Free Nanoparticle}} \times 100$$

From the Fig.15, it was found that the amount of encapsulated nanoparticle= 4.1125 mg and the amount of encapsulated+ free nanoparticle= 5 mg (amount of nanoparticle present in the liposome initially). By applying these values in the above formula the encapsulation efficiency was calculated as 82.25%. This high encapsulation efficiency is mainly because, the silver nanoparticle is poorly soluble in an aqueous medium which facilitated them to incorporate in the hydrophobic part of the liposome. Also, there is an adequate space both in the lecithin and cholesterol for the binding of silver nanoparticles because of the suitable ratio between lecithin, cholesterol, and silver nanoparticles, which increased the encapsulation efficiency (Nayyer *et al.*, 2019).

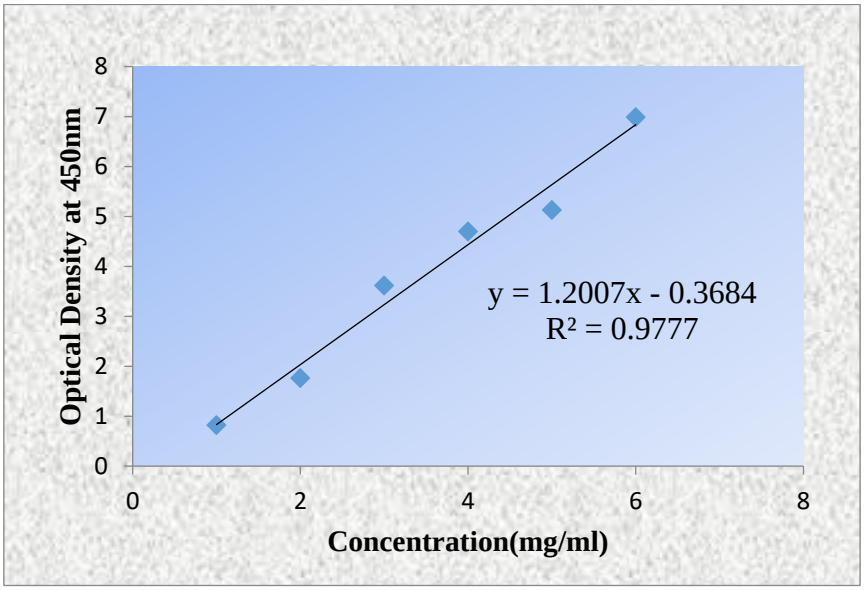

Fig. 15: Encapsulation efficiency of silver nanoparticles loaded liposomes

The encapsulation efficiency of herceptin conjugated liposomes loaded with Simvastatin and Doxorubicin was found to be 81.7% and 84.32% respectively (Li et al., 2019). In line with our study Hardiansyah et al., (2017) loaded curcumin in both PEGylated magnetic liposomes and PEGylated and found that the PEGylated liposomes possess high encapsulation efficiency of curcumin ($78.06 \pm 0.57\%$) than PEGylated magnetic liposomes ($76.15 \pm 1.6\%$). The curcumin was encapsulated in the liphophilic part of the lipid bilayer of liposome. Najlah *et al.*, (2019)

developed disulfiram encapsulated PEGylated liposome which showed an encapsulation efficiency of more than 80%. Similar observations were recorded by Ng *et al.,* (2018) who prepared curcumin and salbutamol loaded liposomes and found that the encapsulation efficiency was 81.1% and 88.6% respectively. This high encapsulation efficiency was attained due to the suitable ratio of lipid and the drug to be encapsulated.

From the results of the current study, it may be concluded that the high encapsulation of silver nanoparticles into the liposomes is due to the suitable ratio of lipids and nanoparticles, adequate incubation period and also suitable composition of the lipids.

4.1.5.2. FTIR Analysis

FTIR is a conventional technique that is widely used by the researchers and industrialists for analysing composition and structure of the molecules. It is a fast and reliable tool that is used to identify the functional group of the substances. FTIR is a reflectance and absorption spectroscopy in the infrared region. This technique is widely used by the researchers for the characterisation of materials (Fahelelbom *et al.,* 2022).

The FTIR spectral analysis was done for various samples like Hydroethanolic extract, silver nitrate, silver nanoparticles, liposome blank and silver nanoparticles loaded liposome to analyse the functional groups present in them, and the FTIR pattern was given in the following figures. The FTIR spectrum of Hydroethanolic extract reveals various peaks which correspond to the following functional groups: a peak at 501.49 cm^{-1} corresponds to the C-I stretching of Halo Compound, various peaks at 563.21 cm^{-1}, 601.79 cm^{-1}, and 678.94 cm^{-1} corresponds to C-Br stretching of Halo Compounds. An FTIR spectrum at 879.54 cm^{-1} indicates C=C bending of Alkenes. A peak at 1041.56 cm^{-1} corresponds to CO-O-CO stretching of Sulfoxide. Peaks at 1080.14cm^{-1} and 1273.02 cm^{-1} indicate C-O stretching of Primary Alcohol and Alkyl Aryl Ether respectively. Another peak at 1381.03 cm^{-1} indicates O-H bending of phenolic compounds. A peak at 1643.35 cm^{-1} indicates C=C stretching of Alkene. Peaks at 2900.94 cm^{-1} and 2973.09 cm^{-1} represent C-H stretching of Alkane groups. An FTIR spectrum at 3317.56 cm^{-1} represents C-H stretching of Alkyne group.

The FTIR spectrum of silver nitrate produces various peaks which correspond to the following functional groups: peaks at 555.50 cm^{-1} and 601.79 cm^{-1} correspond to C-I stretching of Halo Compounds. An FTIR peak at 678.94 cm^{-1} indicates C-Br stretching of Halo Compound. A peak at 1342.46 cm^{-1} represents C-H bending of Alkanes. Another peak at

1635.64 cm^{-1} the C=C stretching of Alkene. An FTIR peak at 3302.13 cm^{-1} corresponds to C-H stretching of Alkyne groups.

The FTIR spectrum of green synthesized AgNP of *Tabebuia pallida* produces various peaks which correspond to the following functional groups: peaks at 547.78 cm^{-1} and *594.08* cm^{-1} represent C-I stretching of Halo Compound. A peak at 671.23 indicates C-Br stretching of Halo Compound. Peaks at 702.09 cm^{-1} and 948.98 cm^{-1} corresponds to C=C bending of Alkene groups. An FTIR spectrum at 1018.41 cm^{-1} represents CO-O-CO stretching of an Anhydride group. Another peak at 1311.59 cm^{-1} indicates C-O stretching of Aromatic Ester. 1411.89 cm^{-1} represents S=O stretching of Sulfonyl Chloride groups. A peak at 1435.04 cm^{-1} indicates O-H bending of Carboxylic Acid functional group. Another peak at 1658.78 cm^{-1} C=C stretching of Alkene groups. An FTIR spectrum at 2600.04 cm^{-1} represents S-H stretching of Thiol group. Peaks at 2916.37 cm^{-1} and 3001.24 cm^{-1} represent C-H stretching of Alkane and Alkene respectively. A peak at 3402.43 cm^{-1} indicates N-H stretching of Aliphatic Primary Amine group.

The FTIR spectrum of liposome blank (lecithin and cholesterol alone) or unloaded liposome produces various peaks which correspond to the following functional groups: peaks at 555.50 cm^{-1} and 678.94 cm^{-1} represent C-Br stretching of halocompounds. An FTIR spectrum at 601.79 cm^{-1} indicates C-I stretching of halocompounds. Various peaks at 948.98 cm^{-1}, 1010.70 cm^{-1} and 1635.64 cm^{-1} indicates C=C bending and stretching of Alkene groups. Another peak at 3363.86 cm^{-1} represents O-H stretching of Alcohol.

The FTIR spectrum of silver nanoparticles loaded liposomes represents various peaks which correspond to the following functional groups: FTIR peaks at 501.49 cm^{-1} and 594.08 cm^{-1} represents C-I stretching of Halo Compounds. A peak at 756.10 cm^{-1} represents C=C bending of Alkene group. An FTIR spectrum at 1056.99 cm^{-1} indicates S=O stretching of Sulfoxide groups. A peak at 1219.01 cm^{-1} represents C-O stretching of Vinyl Ether. An FTIR band at 1373.32 cm^{-1} indicates S=O stretching of Sulfonate groups. A peak at 1458.18 cm^{-1} indicates C-H bending of Alkane group. An FTIR band at 1735.93 cm^{-1} indicates C=O stretching of Aldehyde group. Peaks at 2854.65 cm^{-1} and 2924.09 cm^{-1} corresponds to C-H stretching of Alkane group. A peak at 3387.00cm^{-1} represents N-H stretching of Aliphatic Primary Amines.

The FTIR study reveals the involvement of various functional groups that is responsible for the formation of silver nanoparticles and silver nanoparticles loaded liposomes. These functional groups of the active metabolites are responsible for the various therapeutic potential of the AgNPs and AgNPs loaded liposomes.

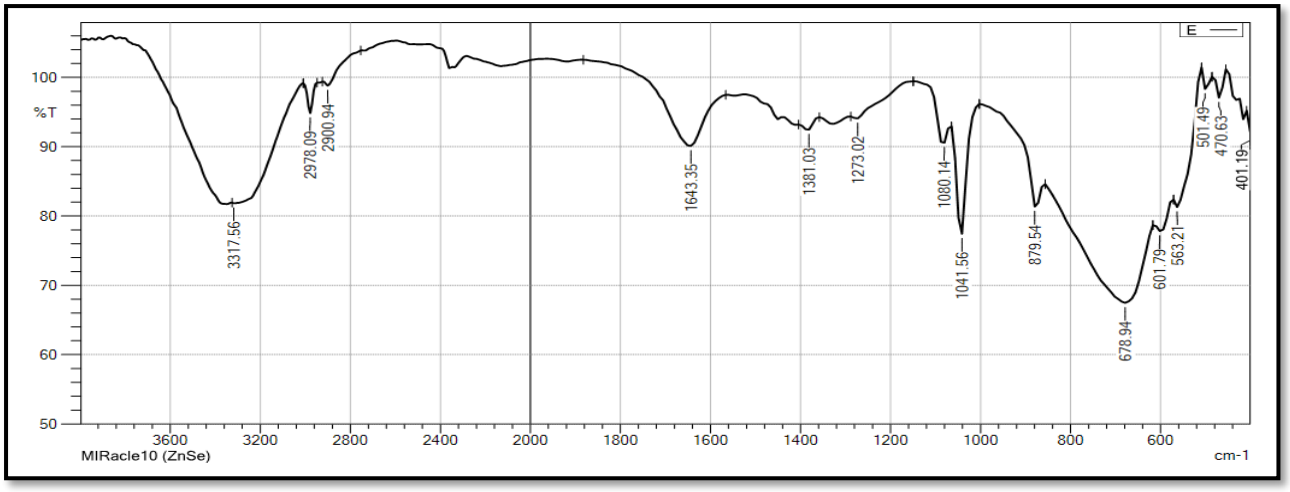

Fig. 16: FTIR spectral analysis of Hydroethanolic extract of *Tabebuia pallida*

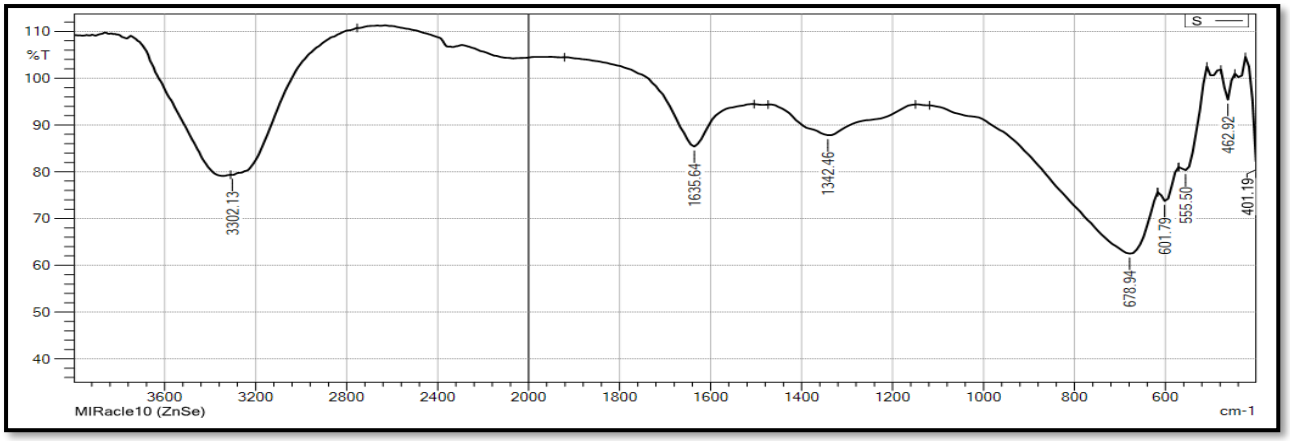

Fig. 17: FTIR spectral analysis of silver nitrate

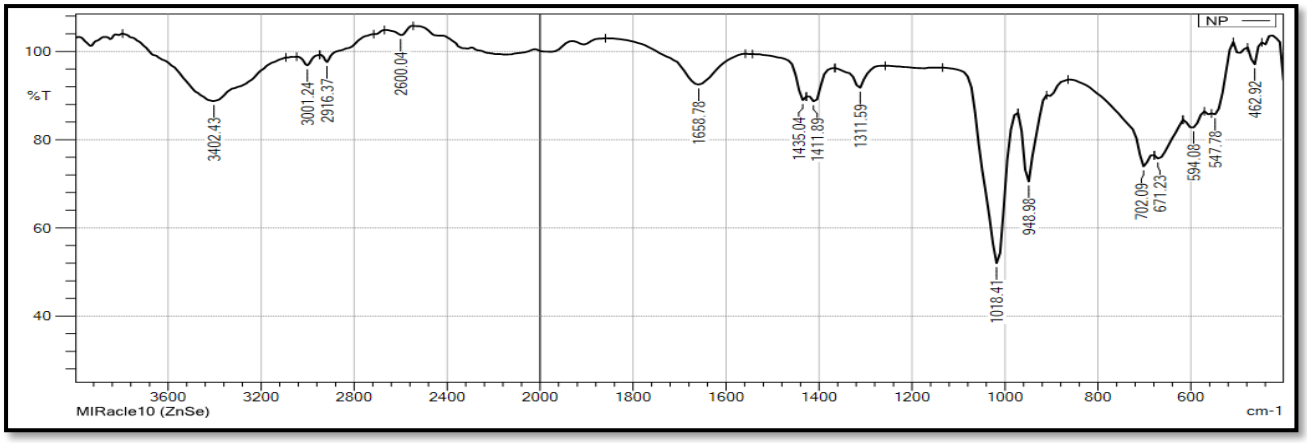

Fig. 18: FTIR spectral analysis of green synthesized *Tabebuia pallida* silver nanoparticles

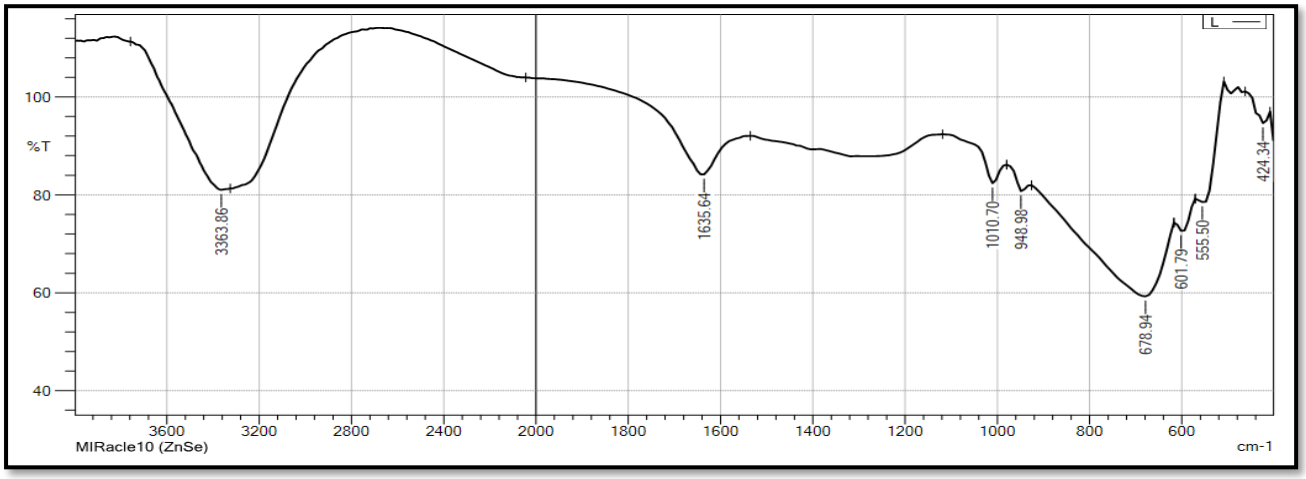

Fig. 19: FTIR spectral analysis of blank liposomes

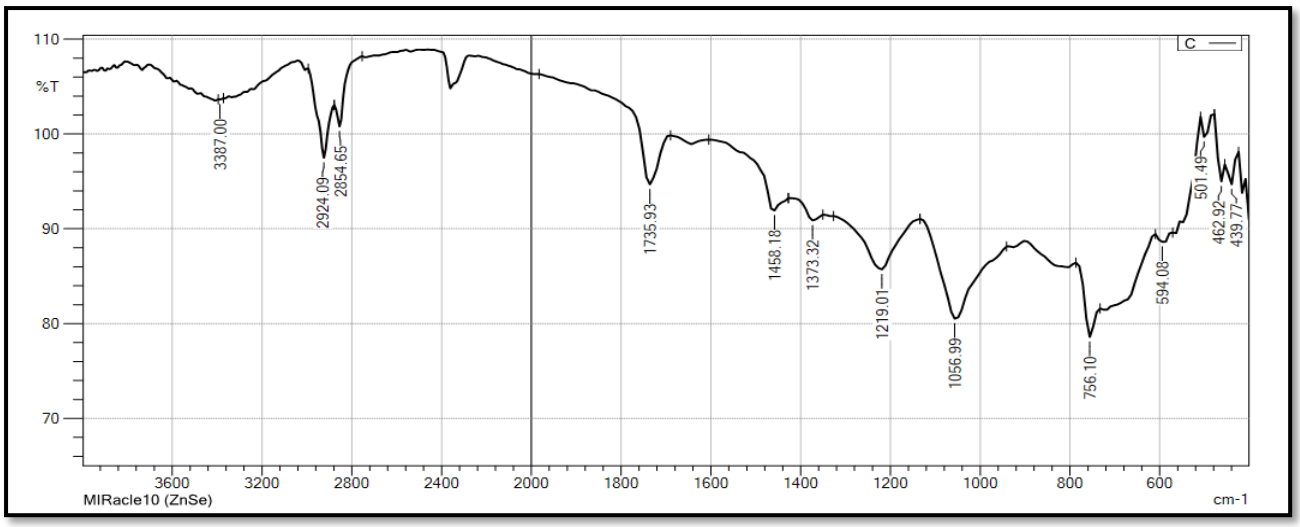

Fig. 20: FTIR spectral analysis of *Tabebuia pallida* silver nanoparticles loaded liposomes

In accordance with our findings Vinodhini *et al*., (2022) synthesized silver nanoparticles from *Tabernaemontana divaricate*, *Basella alba*, and *Allium fistulosum* extracts and analysed their functional groups by FTIR analysis and stated that various functional groups available in the plant extracts acted as capping agents and are involved in the production of silver nanoparticles. Sumaiya *et al*., (2022) carried out green synthesis of AgNPs using *Alhagi graecorum* leaf Extract and reported that the plant extract is complex in nature with number of functional groups present and when the it is allowed to reduce the silver nitrate to silver nanoparticles there is a drastic reduction in the functional groups which indicates the purity of the synthesized nanoparticles. In line with our study, Chandrasekharan *et al., (*2022) synthesized silver nanoparticles using *Gmelina arborea* extract and found that various functional groups are employed in the process of reduction which includes alcoholic groups, hydroxyl flavonoids, carbonyl or carboxylic groups, phenolic and amino groups. These functional groups act as capping agent during the formation of silver nanoparticles and also involved in the stabilization of the synthesized nanoparticles. Yosra *et al.,* (2022) prepared natural extracts-loaded food grade nanoliposomes and analyzed the functional groups present in both blank liposomes and the liposomes loaded with natural extracts and found that there is a structural change between the blank liposome and drug loaded liposome which confirms the encapsulation of drug into the lipid bilayer. Similar results were observed by Wang *et al.,* (2021) who prepared blueberry anthocyanin liposomes and analyzed the presence of functional groups by FTIR analysis and found that the interaction between the functional groups of liposomes and the anthocyanin made the encapsulation possible. The hydrogen bonding or hydrophobic interaction makes the encapsulation of anthocyanin into the liposomes strong.

From FTIR results, it is evident that the different functional groups available in the Hydroethanolic extract are employed in the reduction of silver nitrate to silver nanoparticles and also acted as reducing agents thereby improving the stability of the synthesized nanoparticles. The functional group changes between the blank liposomes and the silver nanoparticles loaded liposomes indicate the successful encapsulation of silver nanoparticles of *Tabebuia pallida* into the liposomes.

4.1.5.3. Field Emission Scanning Electron Microscope

FESEM is used to analyze morphology, size, aggregation and also nanoparticles distribution. The image is generated as a result of reflection of electrons by the samples. It produces the images of nanoparticles at very high resolution (Gupta *et al.* 2019). From the

FESEM analysis of *Tabebuia pallida* silver nanoparticles, it was observed that the size of the nanoparticles ranges from 31.76-50.36 nm and the mean size of the synthesized nanoparticles is observed to be 38.82 nm and are spherical in shape. The size of the silver nanoparticles loaded liposomes were found to be ranging between 80.69-99.71 nm and the average size is found to be 88.11 nm and are also spherical in shape (Fig. 21a and 21b).

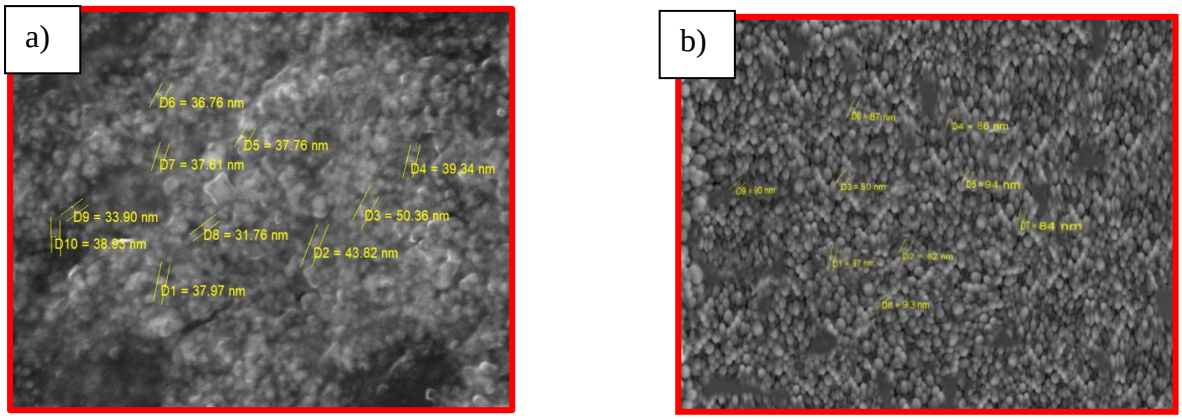

a- FESEM image of silver nanoparticles, b-FESEM image of silver nanoparticles loaded liposomes

Fig. 21: FESEM analysis of silver nanoparticles and silver nanoparticles loaded liposomes of *Tabebuia pallida*

A study carried out by Shah *et al.,* (2021) reported the presence of spherical silver nanoparticles with the average size of about 30±4 nm, synthesized using *Plantago lanceolata* extract. The FESEM analysis of silver nanoparticles from *Azadirachta indica* indicates the formation of spherical shaped AgNPs with the average particle diameter of about 33.20±3.79 nm (Chinnasamy *et al.,* 2021). Similar results were observed by Santhoshkumar *et al.,* (2021) who synthesized the silver nanoparticles from aqueous leaf extracts of *Piper colubrinum* and carried out SEM analysis and interpreted that the size of the synthesized AgNPs ranges between 10 to 50 nm and are spherical. The FESEM micrographs of the turmeric extract loaded nanoliposomes revealed that the synthesized liposomes are uniformly spherical in shape with the size ranges between 74 to 101 nm (Karimi *et al.,* 2019). In another study carried out by Lujan *et al.,* (2019) observed uniformly distributed spherical miRNA loaded liposomes with homogenous size.

The present study results are in accordance with the above mentioned literatures. From the results of the present study, it can be concluded that the spherical shaped silver

nanoparticles and silver nanoparticles loaded liposomes of varying sizes are evident from the micrographs of FESEM.

4.1.5.4. Dynamic Light Scattering:

DLS is a light scattering technique that measure the size distribution and size of the particles. It is widely used to characterize nanoparticles and liposomes. This technique is used to measure the mean size of the particles that are in liquid phase as it is based on Brownian motion. The size of the nanoparticles and liposomes measured using DLS will be slightly larger than the size determined by SEM analysis as SEM only measures the number based size distribution but it will not include the capping agent. But DLS is based on the measurement of hydrodynamic size of the particle which measures the size of the particles along with the ions that are attached on the surface of the particle (Malm and Corbett, 2019 and Almatroudi, 2019). Another parameter that should be considered in DLS analysis is Polydispersity index (PDI). If the PDI value is found to be more than 0.5, it indicates that the particles will get aggregated easily (Nayak *et al.*, 2017).

The DLS pattern of the present study reveals that the silver nanoparticles synthesized using *Tabebuia pallida* leaves has an average size of 55.4 nm with the PDI of 0.33 (Fig.22a). The silver nanoparticles loaded liposomes are found to possess an average size of about 172.1 nm with 0.381 polydispersity index (Fig. 22b). The silver nanoparticles and silver nanoparticles loaded liposomes possess PDI value less than 0.5 which clearly indicates their non- aggregating property.

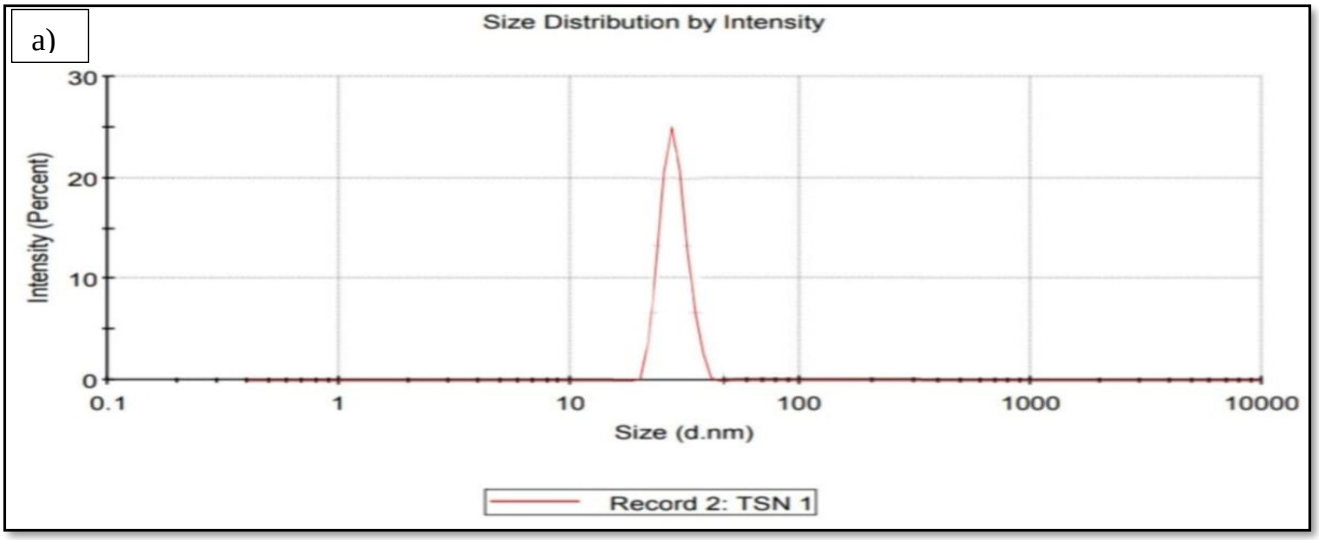

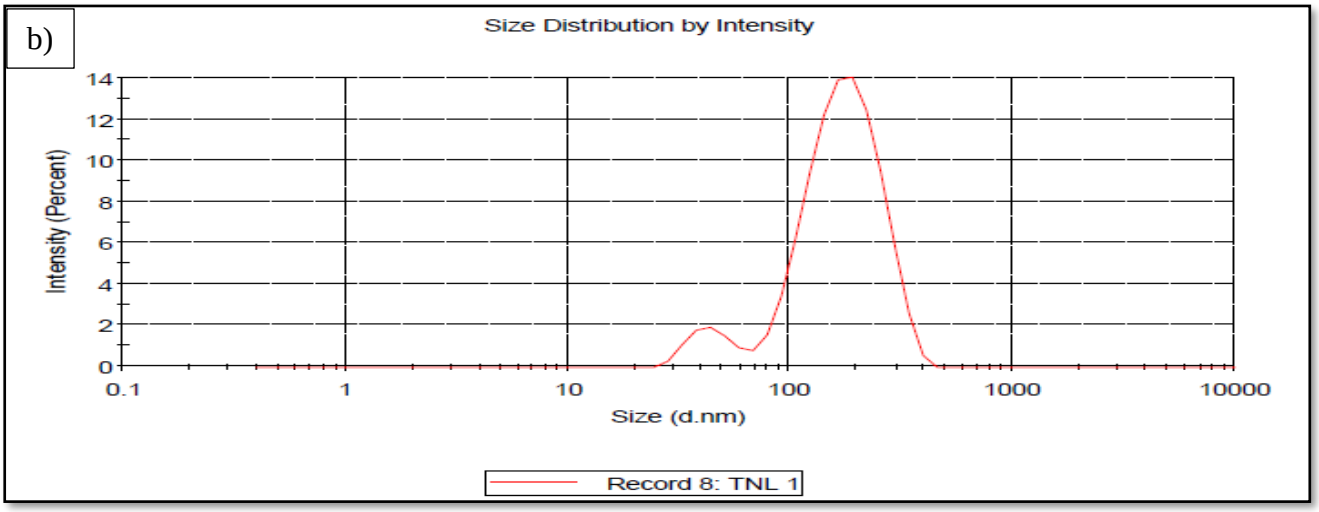

a-DLS pattern of silver nanoparticles of *Tabebuia pallida*, b- DLS pattern of *Tabebuia pallida* silver nanoparticles loaded liposomes

Fig. 22: DLS analysis of silver nanoparticles and silver nanoparticles loaded liposomes of *Tabebuia pallida*

The Dynamic light scattering data of the Walnut green husk mediated silver nanoparticles represent the particle size of about 51nm with a polydispersity index of 0.4. The PDI value obtained in this study is accepted as it provides non-aggregating potential (Khorrami *et al.,* 2018). The uniformly distributed AgNPs with the mean size of 57 nm are obtained using *Persea Americana* bark extract (Francois *et al.,* 2019). The mean size distribution of the AgNPs synthesized using the plant gums of *Prosopis chilensis*, *Azadirachta indica* and *Araucaria heterophylla* was found to be 50nm (Samrot *et al.,* 2019). Yao *et al.,* (2021) synthesized triple responsive targeted hybrid liposomes by conventional thin film hydration method and observed that the mean size of the synthesized liposomes was found to be 166.6nm and 168.8 nm which facilitate the accumulation of liposomes in the tumor site. The Polydispersity index was observed to be 0.27 and 0.25. Cheng *et al.,* (2019) synthesized Doxorubicin loaded liposomes to target breast cancer cells. One of their formulations exerted the average particle size of about 172 nm.

From the above literatures and results obtained in our study it could be assumed that synthesized silver nanoparticles and silver nanoparticles loaded liposomes of *Tabebuia pallida* leaf extract possess optimum size for the uptake by the cancer cells and their Polydispersity

index represents their non- aggregating nature which facilitates their long term stability and found as a suitable drug carrier.

4.1.5.5. Zeta potential

The Zeta potential analysis is carried out to analyze the surface charge and colloidal stability of the synthesized AgNPs and AgNP loaded liposomes. When the electric field is applied, the particles in solution move either towards the positive or negative electrode which determines the velocity of the particles *(Silva et al., 2019).* The value of zeta potential may either have high negative value or high positive value which makes them repel each other and prevent them from agglomeration. On the other hand, the low negative and positive zeta potential indicates that the particles are highly prone to agglomerization. This high negative or positive zeta potential provides long term stability to the particles (Sharma *et al.,* 2022).

The zeta potential of the green synthesized *Tabebuia pallida* silver nanoparticles was -15.6 mV and for the silver nanoparticles loaded liposomes, it was seen to be -21.5 mV (Fig). This high negative zeta potential clearly indicates that the synthesized AgNPs and AgNPs loaded liposomes are highly stable since the particles in the solution repel each other and exist for a longer time with least agglomeration. The stability of AgNPs is found to be enhanced after loading it into the liposomes which is clearly evident from the increase in negative zeta potential.

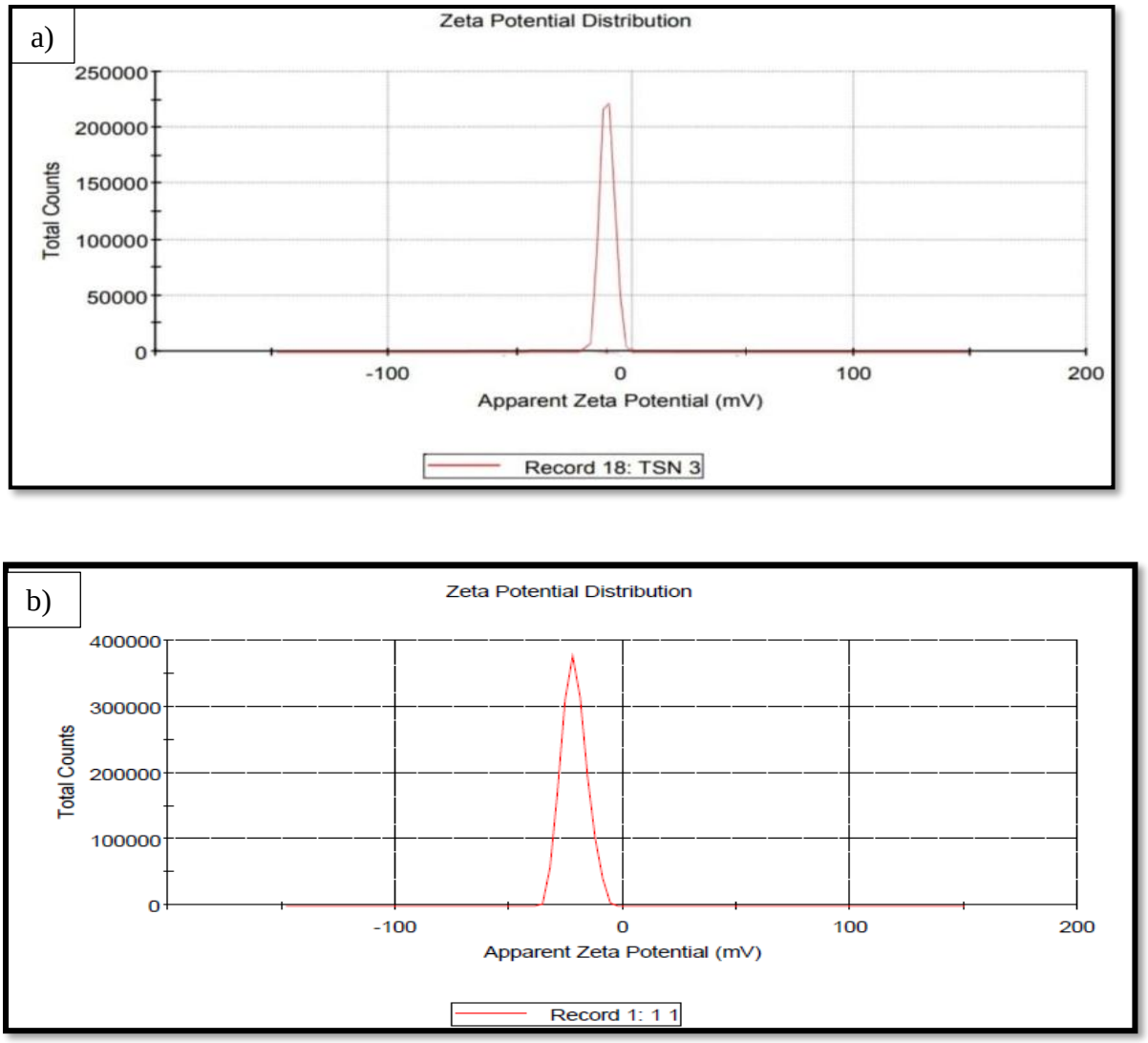

a- Zeta potential of AgNPs, b- Zeta potential of AgNPs loaded liposomes

Fig. 23: Zeta potential of silver nanoparticles and silver nanoparticles loaded liposomes of *Tabebuia pallida*

Similar findings were observed by Ahmed *et al.*, (2022) who synthesized AgNPs from the leaf extract of *Salsola vermiculata* and observed that the zeta potential of the AgNPs was −14.33 ± 0.6 mV. A higher zeta potential is observed which indicates the stability of the nanoparticles. In accordance with our study Joel *et al.*, (2020) synthesized AgNPs using *Aloe vera* gel extract and loaded them into the liposomes made of phosphatidyl choline and cholesterol. From their study, it was observed that the zeta potential of the AgNPs was initially -18.96 mV and found to be increased to around -40 mV. This increase in zeta potential after encapsulation into the liposomes ensures the greater stability of the silver nanoparticles. Yusuf and Casey (2020) carried out chemical mediated synthesis of silver nanoparticles and

encapsulated it into the liposomes and observed that there is an increase in the value of zeta potential before and after encapsulation of silver nanoparticles into the liposomes. Initially the zeta potential of the AgNPs was − 25.7 mV and after encapsulation it escalated to − 30.8 mV. They concluded that this increase in zeta potential increases the stability of AgNPs. Marcela *et al.,* (2020) synthesized silver nanoparticles using *Arctium lappa* and encapsulated it into the liposomes. The zeta potential of the AgNPs was found to be -17 mV and for silver nanoparticles loaded liposomes, it was found to be -20.45 mV. This increase in zeta potential is due to the fact that the encapsulation of silver nanoparticles into the liposomes increases the stability of the AgNPs.

Thus, the present study results could be concluded that the stability of both silver nanoparticles and silver nanoparticles loaded liposomes are high which could be due to the high negative zeta potential, and also there is an increase in zeta potential when the silver nanoparticles are loaded into the liposomes when compared to its free form which clearly indicates that the encapsulation increases the stability of AgNPs.

Phase II

After green synthesizing silver nanoparticles using *Tabebuia pallida* leaf extracts and the stable liposome carrier, it becomes essential to study the drug release profile of AgNPs loaded liposomes.

4.2. Evaluation of Drug Release profile of AgNPs Loaded Liposomes

Liposomes are spherical vesicles made up of lipid bilayer. They are used extensively as a carrier to deliver a variety of therapeutic drugs to the targeted site. They can deliver both hydrophilic and hydrophobic drugs since they have the compartment to entrap both the kind of drugs (Saraf *et al.*, 2020). The liposomes initially bind with the lipid bilayer of the targeted cell and release the encapsulated *Tabebuia pallida* nanoparticles to the cytoplasm of the cell. The lipid nanovesicles are now widely used to deliver a variety of anticancer drugs which paved a new way to treat cancer with minimal side effects (Raj *et al.*, 2019).

4.2.1. *In vitro* drug release study

The *in vitro* release of silver nanoparticles from the liposomes were analyzed using three different pH; pH 7.4 which corresponds to the pH of blood, pH 6.8 which corresponds to the pH of cancer cells and pH 5.5 which corresponds to the mature endosomes of cancer cells for different time intervals like 2, 4, 8, 12, 24, 48 and 72 hours. The *in vitro* drug release profile of silver nanoparticles loaded liposomes are shown in Fig. 24. From the graph,

it was observed that a high silver nanoparticle release from liposomes was observed at pH 5.5 which corresponds to the mature endosomes of cancer cells. The drug release was found to be increased when the time proceeds in all the pH models. 73.32± 0.68 % nanoparticle was released in a time of 72 hours in pH 5.5 system. 22.24± 1.00 % nanoparticle and 20.75± 0.11 % nanoparticle was released at 72nd hour in pH 6.8 and pH 7.4 respectively. A high silver nanoparticle release was observed at low pH and the drug release was found to be decreased when the pH of the system increased. From these evidences, it was confirmed that the drug release was high in acidic conditions. This is because the acidic condition breaks the liposomal integrity and releases the encapsulated silver nanoparticle. This acidic condition promotes the hydrolysis of phospholipids which increases membrane permeability which leads to the release of the encapsulated nanoparticles. However, the liposome structure is resistant to alkali conditions (Jin *et al.,* 2016).

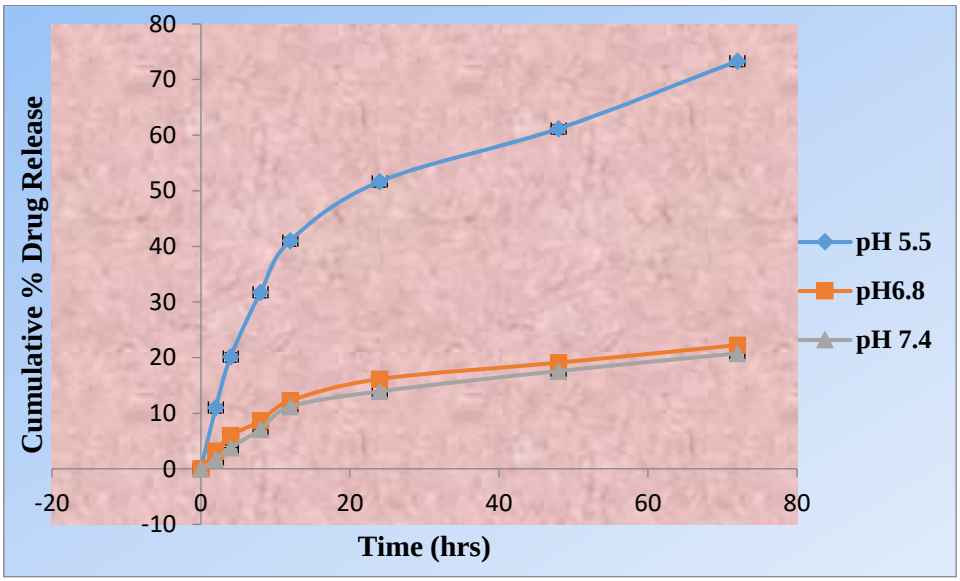

The values are represented as ±SD for triplicates in each category

Fig.24: *in vitro* drug release profile of silver nanoparticles loaded liposomes

Similar findings were indicated by Ankita *et al.*, (2020) who synthesized Paclitaxel and Piperine co-loaded Liposomes and carried out *in vitro* drug release study by dialysis bag method. They have analysed the release of Paclitaxel and Piperine in three different pH 5.5, pH 6.5 and pH 7.4 and observed that there is a high release of the encapsulated drug in pH 5.5. This high release improves the anticancer effect of the drug loaded liposomes thereby diminishing the toxicity to normal cells. In line with our study, Alanood *et al.*, (2018) prepared

afatinib loaded liposomes by thin film hydration method followed by extrusion and carried out drug release analysis in two different pH; pH 5.5 and pH 7.5. They observed a high release of afatinib at pH 5.5 which is the pH that actually mimics the pH of the tumor cells. The tumor cells possess acidic pH since the endosomes and lysosomes are weakly acidic in nature. Nandi *et al.,* (2021), prepared sirolimus-encapsulated liposomes and carried out drug release analysis at pH 6.8 and observed that there is controlled release of the Sirolimus from the liposome. Manju *et al.,* (2019) prepared Dual pH-sensitive liposomes loaded with gemcitabine and carried out drug release analysis in three different pH; pH 5.0, pH 6.5 and pH 7.4 and observed a highest release of gemcitabine at pH 5.0.

Thus from the findings of the *in vitro* drug release analysis of silver nanoparticles loaded liposomes, it is confirmed that the release of AgNPs are high at acidic pH ie (pH 5.5) which is the pH that corresponds to the mature endosomes of cancer cells which reveals the targeted drug delivery nature of the liposomes. High release is attained in acidic pH because the acidic nature breaks the phopholipid bilayer which leads to the release of encapsulated drug. Since the cancer cells are highly acidic in nature, the drugs are released only in the tumor micro environment which prevents undesired side effects.

4.2.2. Application of mathematical models in release kinetics of silver nanoparticles loaded liposomes

4.2.2.1. Zero-order model

According to zero-order drug release kinetics, a drug release from a drug delivery system remains constant per unit time and it is not dependent on concentration. To evaluate the drug release by zero-order model, a graph was plotted between time and cumulative drug release % (Fig. 25). The slope of the graph provides a rate constant for zero order model. The correlation coefficient R^2 can indicate whether the drug follows zero-order model of drug release or not (Dash *et al.,* 2010).

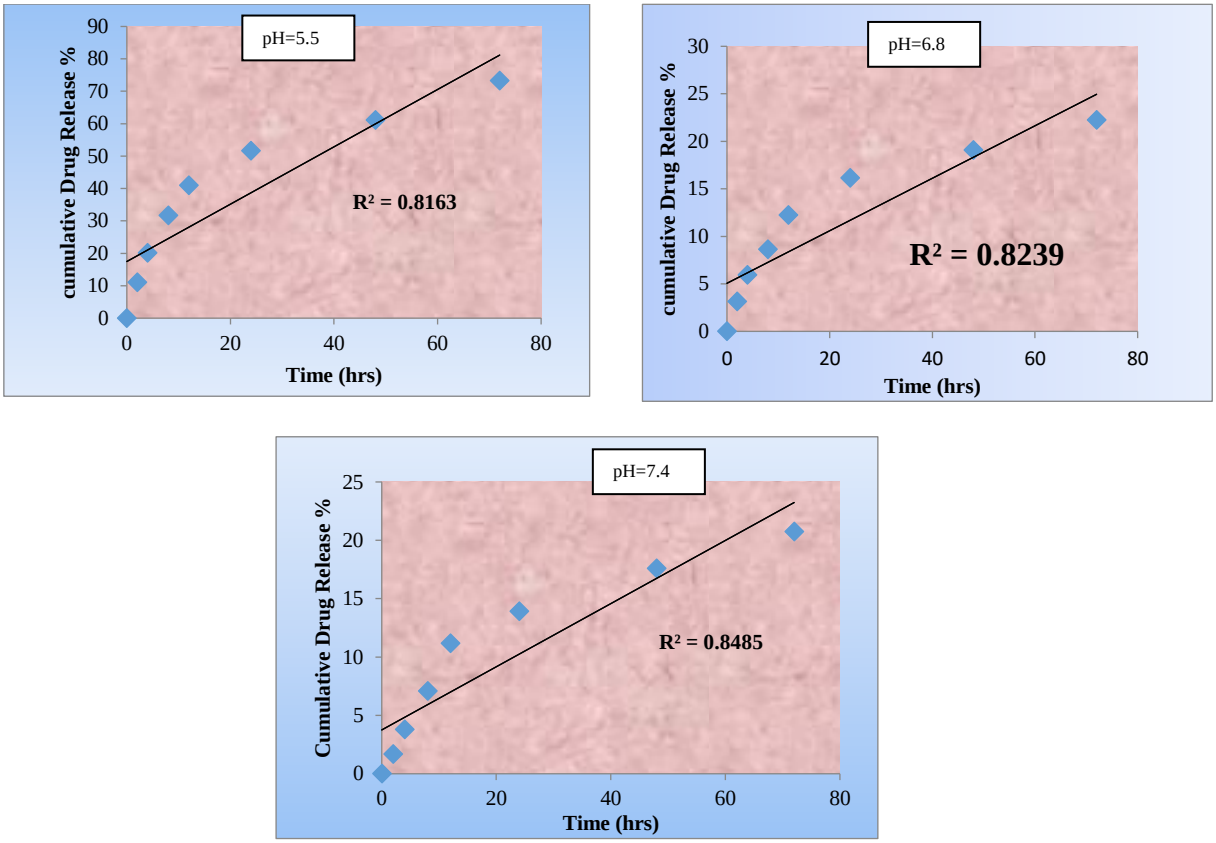

Fig. 25: Zero-order release kinetics

From the above graphs, it could be concluded that the drug release does not follow Zero-order model of release kinetics which is evident from the lower value (R^2=0.816 for pH 5.5, R^2=0.823 for pH 6.8, and R^2=0.848 for pH 7.4) of coefficient of correlation.

4.2.2.2. First-order model

According to First-order drug release kinetics, the release rate of a drug is directly proportional to the concentration of the drug which indicates that when there is a high concentration of drug the release rate also will be high and when the drug concentration decreases the drug release also decreases. (Dash *et al.,* 2010). To study the first-order release kinetics for various pH a graph was plotted between log % of drug remaining and time (Fig.26). From the slope of the line, first-order rate constant can be predicted and the correlation coefficient value indicates whether the release of drug from the system obeys first-order kinetics or not.

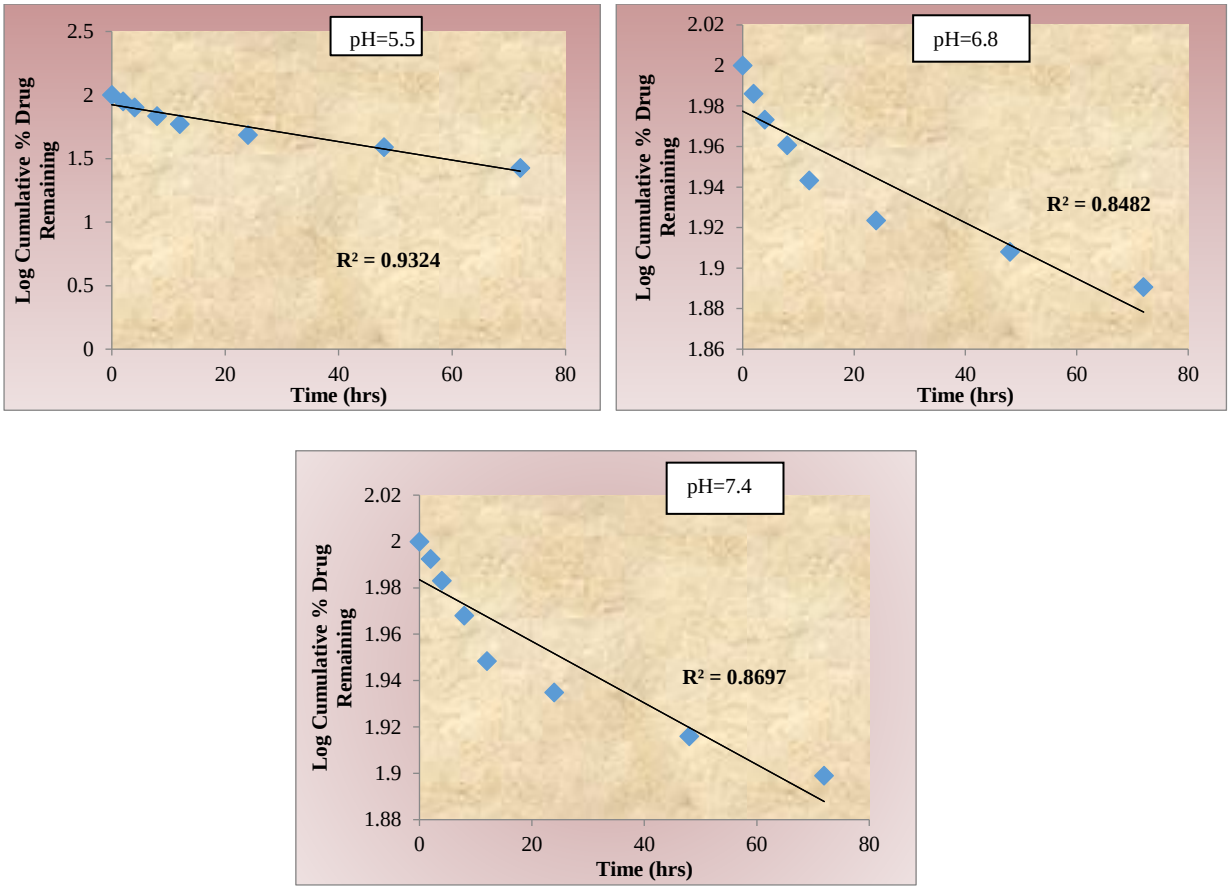

Fig. 26: First order release kinetics

From the above graphs, it could be concluded that the drug release does not follow First order release kinetics as there is a lower value (R^2=0.932 for pH 5.5, R^2=0.848 for pH 6.8, and R^2=0.869 for pH 7.4) of coefficient of correlation.

4.2.2.3. Higuchi model

According to the Higuchi model, the drug release from a matrix as a square root of time is based on the process of diffusion. If there is the highest correlation coefficient then it can be predicted that the drug release is through diffusion. There are some predictions in Higuchi model and they include: the drug concentration is much higher than the solubility of the matrix at time t_0, sink conditions are maintained perfectly and constant drug diffusion (Gouda *et al.*, 2017). To study the Higuchi model of drug release kinetics for various pH, a graph was plotted between Cumulative % drug release and Square root of time (fig. 27)

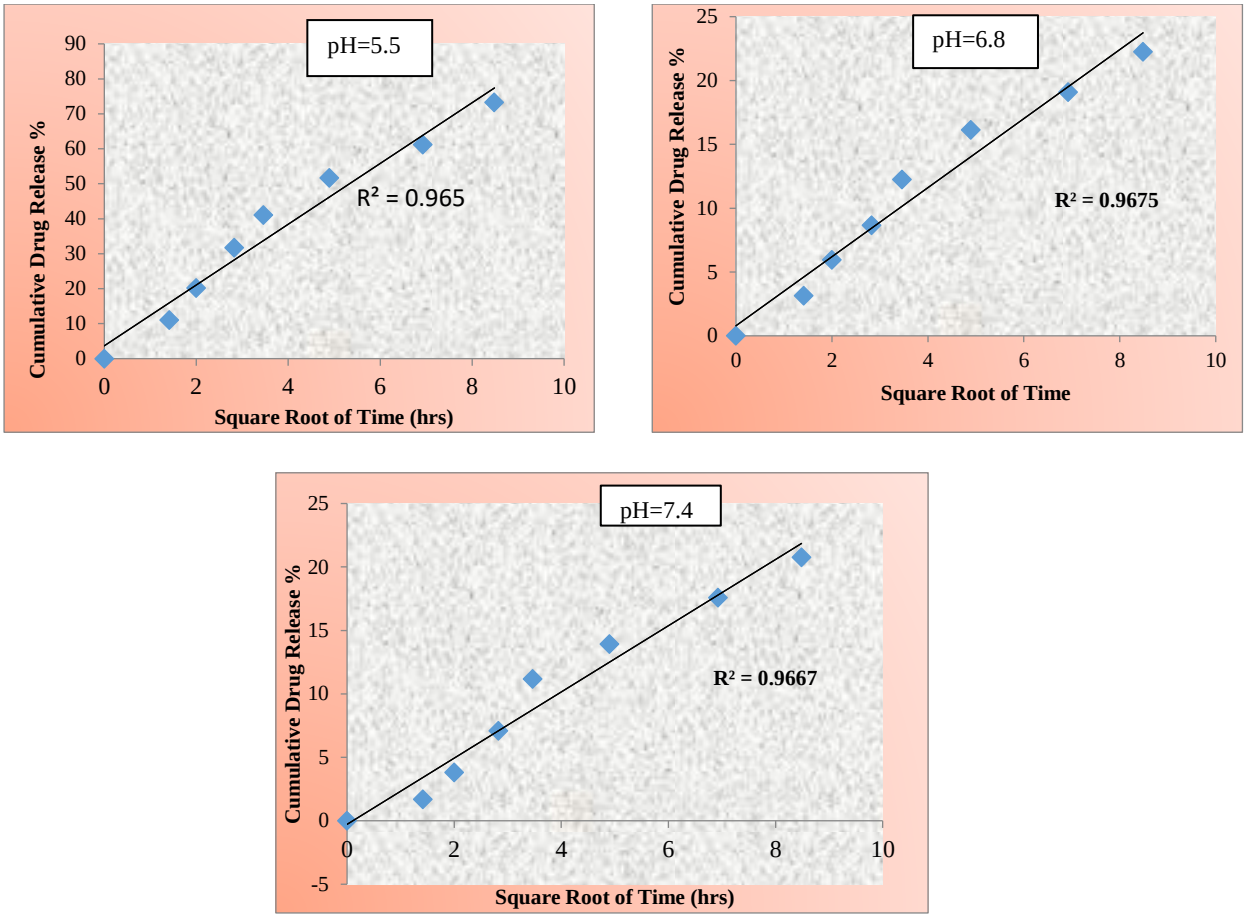

Fig. 27: Higuchi drug release kinetics

From the above graphs, it could be concluded that the drug release perfectly follows Higuchi drug release kinetics as there is the highest value (R^2=0.965 for pH 5.5, R^2=0.967 for pH 6.8, and R^2=0.966 for pH 7.4) of coefficient of correlation. Hence it is clearly evident from the values of correlation coefficient obtained for all the mathematical models analyzed, that the drug is released by the process of diffusion. In order to understand, the type of diffusion the drug undertakes during the drug release process Korsmeyer-Peppas model was also studied.

4.2.2.4. Korsmeyer-Peppas model

From the Higuchi model of drug release kinetics, it is confirmed that the drug release is through diffusion. Korsmeyer-Peppas model is fitted to understand that drug release follows which type of diffusion (Singhvi and Singh, 2011). To study the drug release kinetics by the Korsmeyer-Peppas model, a graph was plotted between log cumulative drug release % and log time (Fig. 28). From the values of release exponent (n) obtained using the plot, the type of diffusion can be predicted.

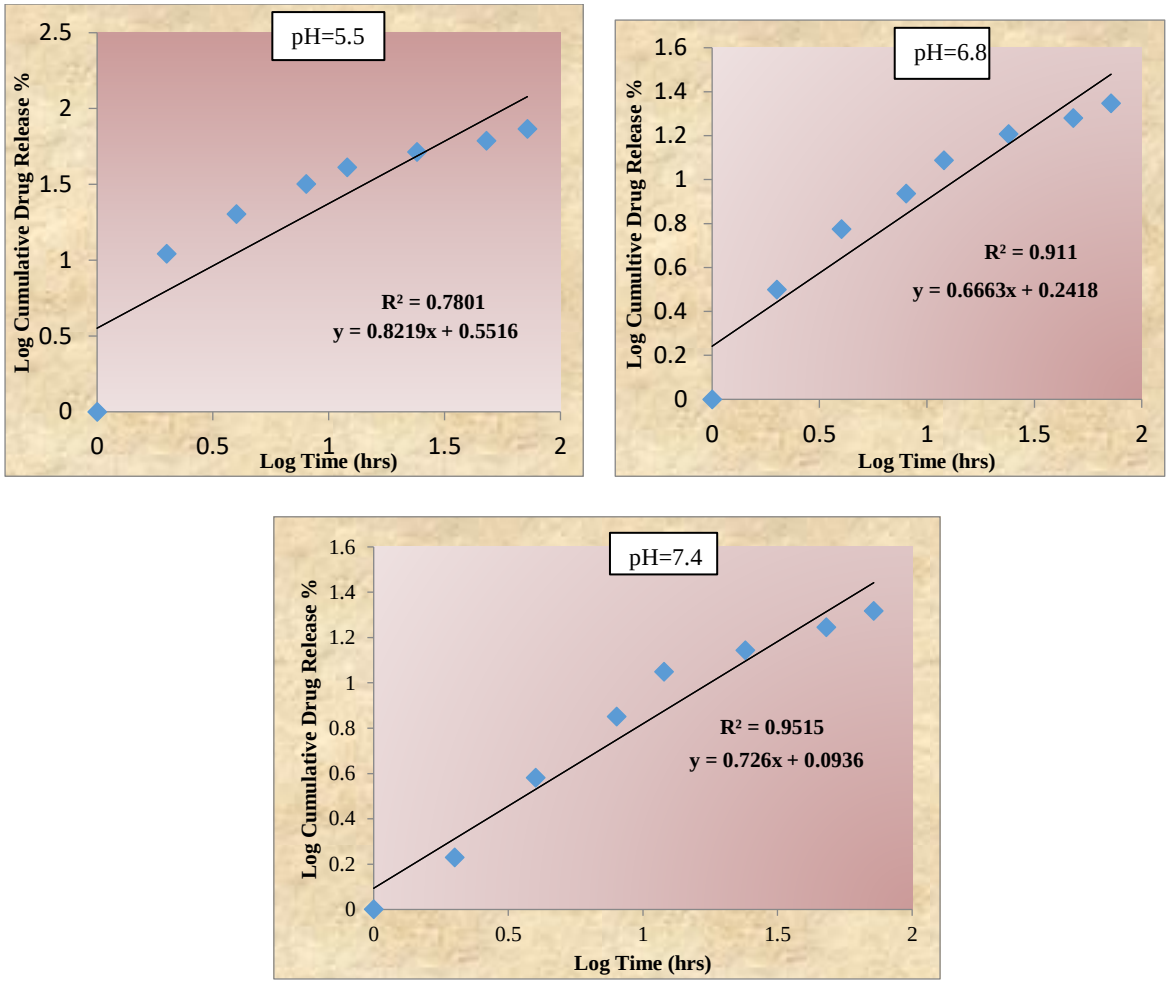

Fig. 28: Korsmeyer-Peppas drug release kinetics

Table 3: Drug transport mechanism based on the values of release exponent (n)

Release exponent (n)	Drug transport mechanism
***n* < 0.5**	Quasi-Fickian diffusion
0.5	Fickian diffusion
0.5 < n < 1. 0	Anomalous (Non - Fickian transport)
1.0	Case II transport
Higher than1.0	Super case II transport

Table 4: Drug transport mechanism for various pH (pH 5.5, pH 6.8 and pH 7.4)

pH	Equation	Release Exponent (n)	Drug Transport Mechanism
5.5	y = 0.821x +0.551	0.821	Non Fickian Transport
6.8	y = 0.666x +0.241	0.666	
7.4	y = 0.726x +0.093	0.726	

The drug transport mechanism depends on the values of release exponent which is given in Table 4. From table 4, it could be concluded, that the drug release for all the pH selected in the present study follow non Fickian transport as their release exponent falls in the category of $0.5 < n < 1.0$ (Padmaa *et al.*, 2018).

4.2.2.5. Hixson-Crowell model

In order to assess whether the drug release is by dissolution as well as diffusion or only by diffusion the Hixson and Crowell model was studied. According to the Hixson-Crowell model, the drug release is by Dissolution and not by Diffusion. It is based on the fact that there is a change in surface area and diameter of the particle when there is dissolution (Singhvi and Singh, 2011). To study the drug release kinetics by Hixson- Crowell model a graph was plotted between cube root of the concentration of drug at time t= 0, and the concentration of drug at time t against time (Fig. 29).

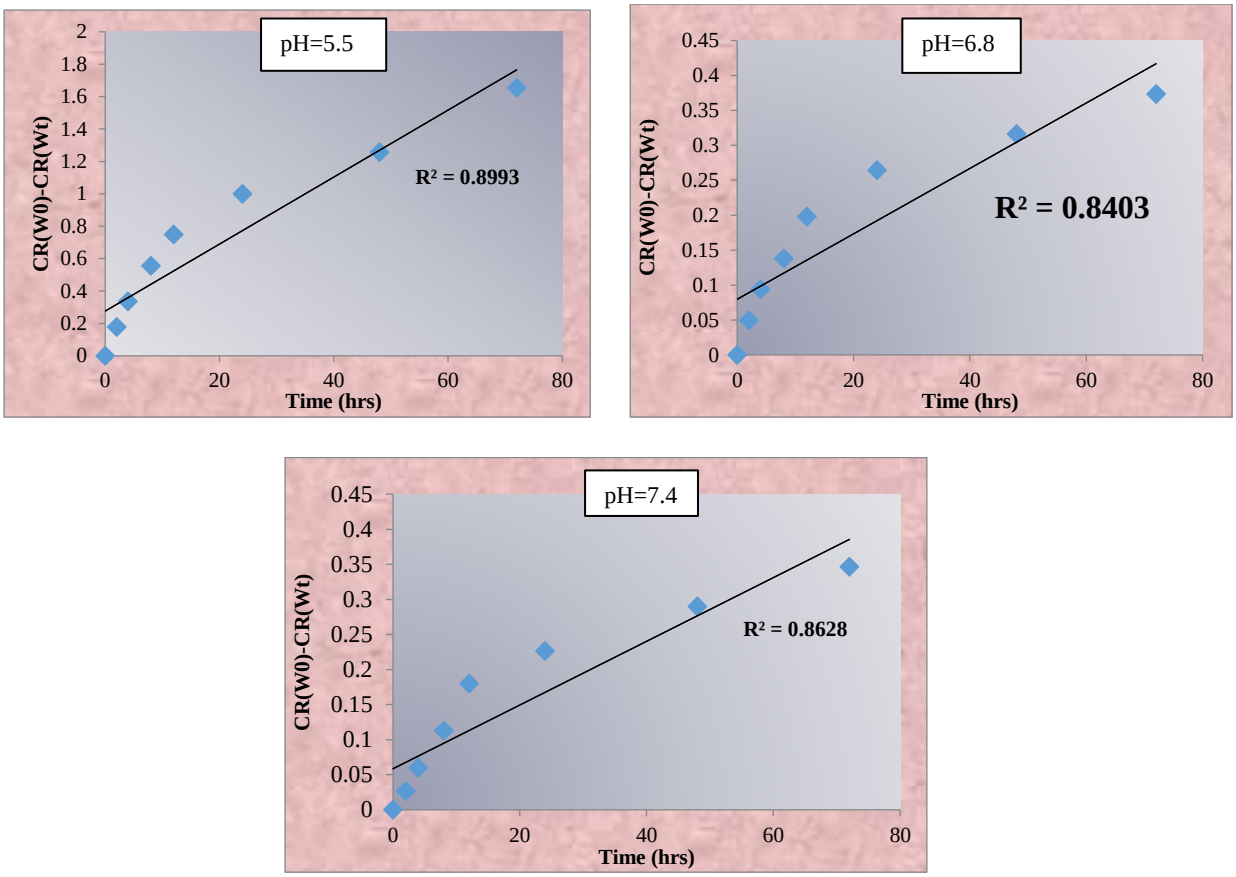

Fig. 29: Hixson-Crowell drug release kinetics

From the above graphs, it could be concluded that the drug release does not follow Hixson-Crowell release kinetics as there is a lower value (R^2=0.899 for pH 5.5, R^2=0.840 for pH 6.8 and, R^2=0.862 for pH 7.4) of coefficient of correlation. The results reiterate the release mechanism involved in the release of silver nanoparticles of *Tabebuia pallida* from the encapsulated liposomes is by diffusion and the drug diffuses when the concentration is high and in the pH range of 5.5 which similar to the tumor environment.

Results of various mathematical models

The *in vitro* drug release profile of AgNPs loaded liposomes were fitted for five different mathematical models and evaluated using correlation coefficient r^2. The results of all five models are given in Table 5. A Suitable mathematical model for *in vitro* drug release study was determined by the highest value of the correlation coefficient (Rescigno, 2003). Among all the models analyzed, Higuchi model was found to be the best suited model as it shows the highest degree of coefficient of correlation. So it could be confirmed that the drug release is

based on diffusion mechanism. From the Korsmeyer-Peppas model, it was confirmed that the drug release is based on anomalous non- Fickian transport.

Table 5: Results of Various mathematical models in terms of r^2, slope, and intercept

Name of the mathematical model	pH 5.5 (Mature Endosomes of Cancer Cells)				pH 6.8 (Cancer Cells)				pH 7.4 (Blood)			
	R^2	Equation	Slope	Intercept	R^2	Equation	Slope	Intercept	R^2	Equation	slope	Intercept
Zero-order	0.816	y = 0.884x +17.47	0.8845	17.474	0.823	y = 0.276x + 5.06	0.2762	5.065	0.848	y = 0.270x +3.754	0.2705	3.755
First-order	0.932	y = -0.007x +1.92	-0.0072	1.923798	0.848	y = -0.001x +1.97	-0.0013	1.977	0.869	y = -0.001x +1.98	-0.0013	1.983
Higuchi	**0.965**	y=8.687x + 3.673	8.6876	3.673744	**0.967**	y = 2.703x +0.789	2.7038	0.789104	**0.966**	y = 2.608x - 0.283	2.6087	-0.28379
Korsmeyer-Peppas	0.780	y = 0.821x +0.551	0.8219	0.551602	0.911	y = 0.666x +0.241	0.6663	0.241776	0.951	y = 0.726x +0.093	0.7259	0.093642
Hixson -Crowell	0.899	y = 0.020x +0.276	0.0206	0.276325	0.840	y = 0.004x +0.079	0.0046	0.079622	0.862	y = 0.004x +0.058	0.0045	0.058526

In line with our study Nayer *et al.,* (2019) prepared turmeric extract loaded nanoliposomes and carried out *in vitro* drug release study and validated the results through various mathematical models, and observed that the Higuchi model was found to be the suitable model as its coefficient of correlation is higher when compared to the other models. Similar findings were observed by Minh *et al.,* (2020), who prepared Letrozole and Paclitaxel loaded liposomes and applied the drug release profile in various mathematical models like, zero-order model, first-order model, Higuchi model, and Korsmeyer-Peppas model, and observed that the Korsmeyer-Peppas and Higuchi models indicated highest correlation coefficient values. Since the release profile of Letrozole and Paclitaxel shows highest correlation coefficient for Higuchi mode it is confirmed that the drug release follows diffusion and also in Korsmeyer and Peppas model the value of release exponent (n) was found to be lower than 0.5 for both *L*etrozole and Paclitaxel which indicates that the drug release follows Quasi-Fickian diffusion. Fateme *et al.,* 2018 prepared PEGylated doxorubicin loaded liposomes and carried out mathematical modeling of drug release kinetics. They observed that the drug release follows Korsmeyer and Peppas model of drug release kinetics. Milad *et al.,* 2012 prepared hesperitin loaded liposomes and analyzed the *in vitro* drug release profiling of the liposomes and validated through different mathematical models. Among the various mathematical models analyzed, the release of hesperitin from the liposomes is found to adhere with Rigter–Peppas model of drug release it has highest value of coefficient of correlation.

In agreement with the above cited literatures and the results obtained from our study it could be concluded that the release of silver nanoparticles from the liposomes follow Higuchi model of drug release as there is a highest value of coefficient of correlation. As the drug release is fitted to Higuchi model, it could be considered that the drug release is through diffusion. From the results of the Korsmeyer-Peppas model, it is considered the drug release is based on the anomalous non- Fickian transport.

The results of phase-II validate characteristics and properties of silver nanoparticles of *Tabebuia pallida* loaded liposomes. The characteristics exhibited by the nanoliposomes reveal that the targeted drug release is highly possible with the prepared nanolioposomes with the nanoparticles of *Tabebuia pallida*.

Phase III:

4.3. Evaluation of Antioxidant Potential of AgNPs and AgNPs Loaded Liposomes

4.3.1. DPPH Radical Scavenging Assay:

2,2-diphenyl-1-picrylhydrazyl is a stable free radical which is used to analyze the antioxidant capacity of the plant samples. The antioxidants present in the samples reduce purple coloured DPPH to a yellow coloured solution which can be measured at 517nm. DPPH assay is widely used as it is reliable, rapid, time consuming, simple and inexpensive (Lalhminghlui and Ganesh, 2018)

The assay was performed using varying concentrations (25, 50, 100, 200, 300, 400 and 500 µg/ml) of hydro ethanolic extract, silver nanoparticles and silver nanoparticles loaded liposomes of *Tabebuia pallida* with quercetin as the standard. The results revealed that all the tested samples and standard were able to scavenge DPPH radical in a dose dependent manner. The samples were able to scavenge the DPPH radical even in the lowest concentration and the scavenging ability was found to be increased when there is an increase in concentration which clearly depicts the dose dependent activity of the samples. Among the tested samples, the silver nanoparticles loaded liposomes were found to possess high DPPH scavenging activity followed by silver nanoparticles and hydroethanolic extract. The half maximum inhibitory concentration (IC50) was also calculated. The IC50 in µg/ml for various samples were as follows: Standard-117.45, Hydro Ethanolic Extract- 440.641, AgNP- 225.67, and AgNP Loaded Liposome-180.1. The IC50 values clearly indicates that the AgNPs loaded liposomes were able to scavenge the DPPH radical effectively when compared to the other samples tested. The results of the DPPH radical scavenging ability clearly indicate that all the samples tested shared its electron to the DPPH radical thereby exhibiting scavenging ability.

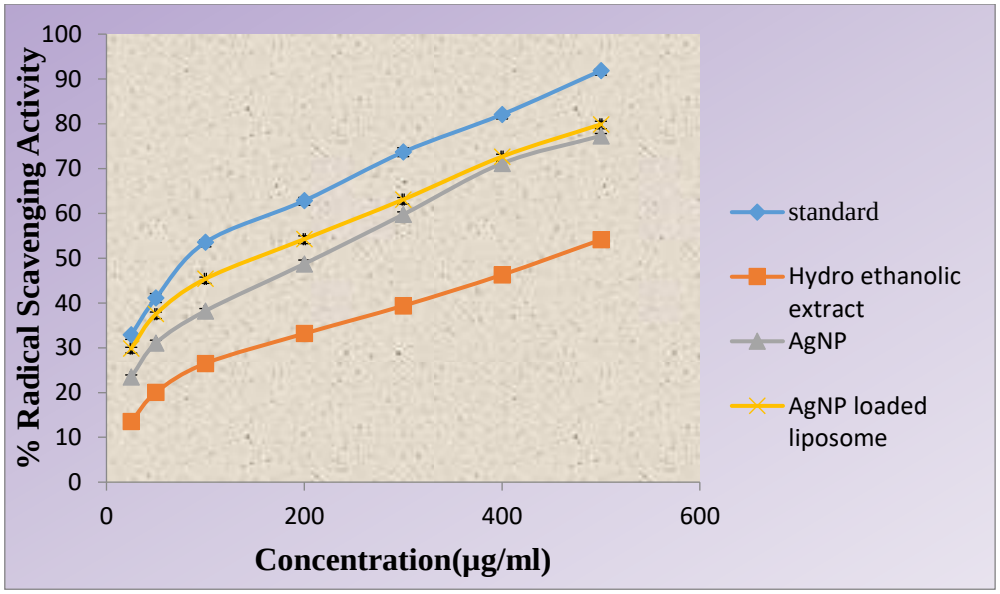

The values are represented as ±SD for triplicates in each category, P< 0.05

Fig. 30: DPPH Radical Scavenging Assay

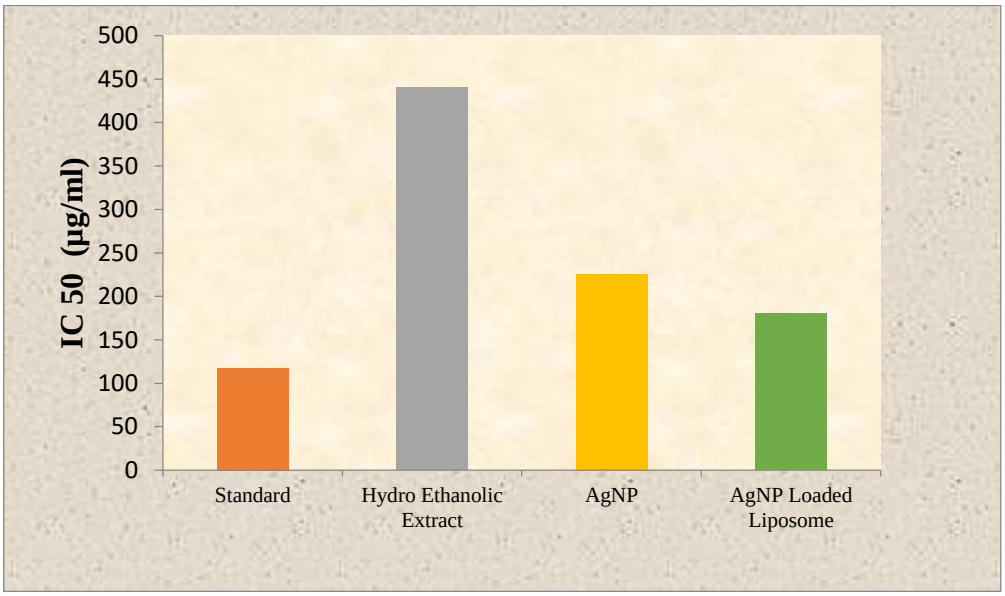

Fig. 31: IC 50 values for DPPH Radical Scavenging Assay

In line with our observations Rahman *et al.*, (2015) prepared methanolic extracts from *Tabebuia pallida* stem bark, root bark, leaves and flowers and carried out DPPH radical scavenging assay and observed that *Tabebuia pallida* leaves possess high antioxidant potential against DPPH radical when compared to the extracts of other parts. The phytochemicals like tocopherol and polyphenol present in the leaf extracts involved in scavenging activity by donating its electrons to the DPPH radical. Jimenez *et al.*, (2018) prepared various solvent extracts of *Tabebuia rosea* leaf and inner bark and found that *T. rosea* leaf ethyl acetate extract

showed highest DPPH scavenging potential when compared to the other extracts of leaf and bark. They suggested that the hydroxyl groups of flavonoids and phenols in the sample are responsible for the scavenging potential. Hemlata *et al.,* (2020) synthesized AgNPs using *C. prophetarum* aqueous leaf extract and analysed its potential to scavenge DPPH radical and found that the synthesized silver nanoparticles are able to scavenge the DPPH radical more than the aqueous extract in a concentration dependent manner. This highest radical scavenging ability of silver nanoparticles is due to the DPPH neutralizing capacity by transferring its electron to the free radical. In a study carried out by Riaz *et al., (*2020), the synthesized AgNPs from ginger extract are more potent against DPPH radical than the ginger extract. This is due to the tendency of the sample to donate proton and also the phytochemicals of the ginger extract that are responsible for the formation of silver nanoparticle. Wang *et al.,* (2022) demonstrated that the DPPH radical scavenging ability of the liposomal anthocyanin was higher than the free anthocyanin. The scavenging ability increases with increase in concentration. This clearly depicts that the liposomes can increase the radical scavenging ability. Our findings are consistent with the results of Rogaie *et al.,* (2016) who studied DPPH radical scavenging activity of both quercetin and quercetin loaded liposomes and found that both the samples showed almost equal potency in scavenging the DPPH radical which clearly indicates that the encapsulation of quercetin into the liposomes doesn't affect its antioxidant potential.

In accordance with the above supporting studies, it is confirmed that all the tested samples donated an electron to the DPPH radical thereby exhibiting scavenging potential. The phenolic compounds, flavonoids and tocopherol present in the leaf extract might be involved in the scavenging activity. The phytochemicals that are present in the AgNPs as capping agent also might play a significant role in scavenging the DPPH radical. The liposomal silver nanoparticles also exhibited scavenging potential which clearly indicates that the encapsulation of silver nanoparticles into the liposomes and doesn't interfere with its radical scavenging ability.

4.3.2. ABTS Radical Scavenging Activity

ABTS is a stable free radical with a maximum absorbance of 734 nm. When the antioxidants are allowed to react with ABTS, there will be a decrease in absorption which is a result of reduction of ABTS by the antioxidants. The reduction is mainly based on the concentration of the antioxidant, and also the time of exposure (Nasreddine et al., 2019).

All the samples tested could exert scavenging action against the ABTS free radical in a concentration dependent manner. The scavenging ability of the samples is in the following order: hydroethanolic extract < AgNP < AgNP loaded liposome < quercetin standard. The results are depicted in the graph below. Among the various samples tested, the silver nanoparticles loaded liposomes are much effective against the ABTS radical which is in par with the standard quercetin. AgNPs loaded liposomes can exert 40% ABTS scavenging even in the lowest concentration (25µg/ml). The ABTS radical scavenging potency of the tested samples is probably due to the electron donating tendency of the phytoconstituents to the free radical.

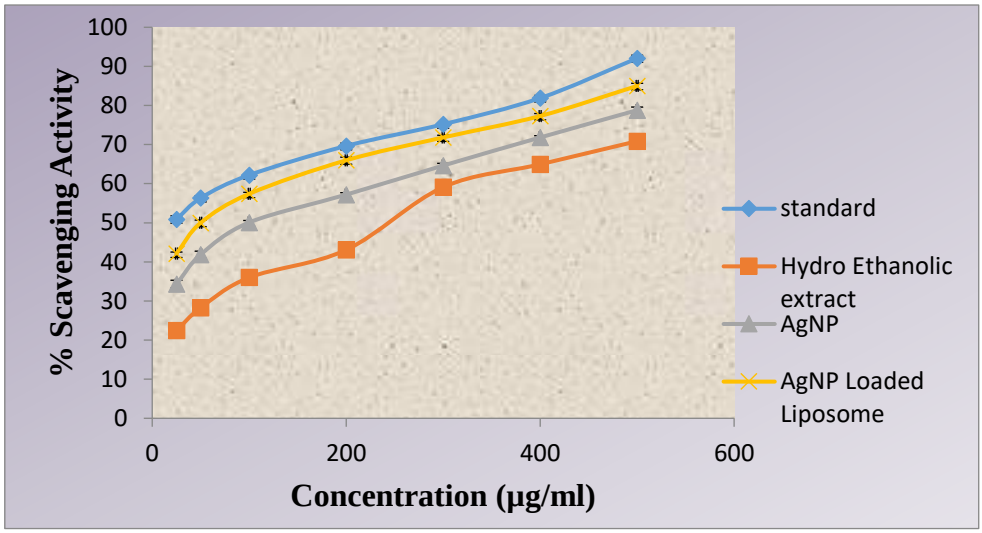

The values are represented as ±SD for triplicates in each category, P< 0.05

Fig. 32: ABTS Radical Scavenging Assay

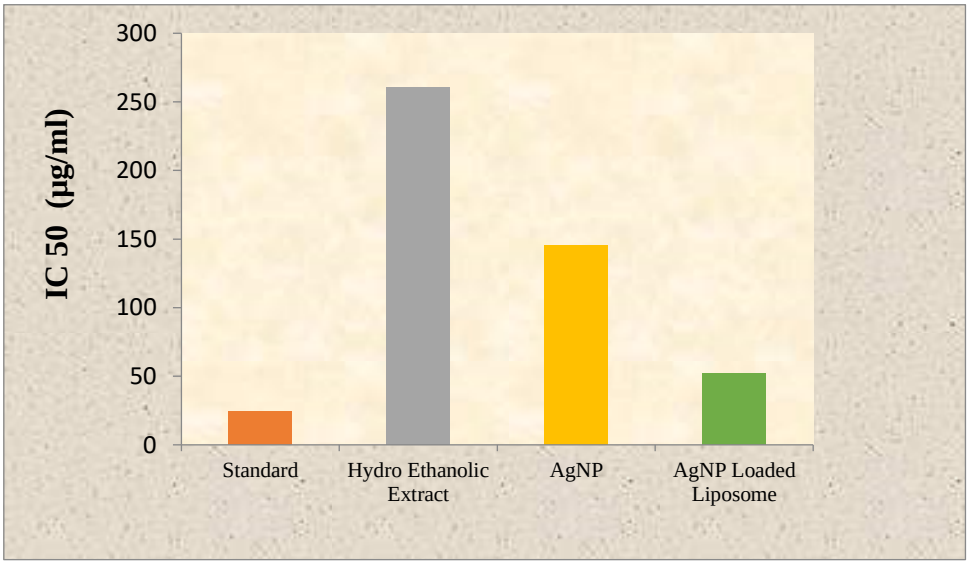

Fig. 33: IC 50 values for ABTS Radical Scavenging Assay

Lalmuansangi *et al.,* (2019) analyzed the antioxidant potential of various solvent extracts of *Mussaenda macrophylla* and found that the extracts can scavenge ABTS radical in a concentration dependent manner. This scavenging potential might be due to the presence of phenolic content in the extracts which donated its electrons to the ABTS radical. According to a study carried out by Jeremiah *et al.,* (2018) the acetone, aqueous, and ethanolic extracts of *Vernonia mespilifolia Less.* exhibited a dose dependent ABTS scavenging potential. This scavenging ability might be due to the presence of various phytoconstituents especially the polyphenolics available in the extracts. Xiaoping *et al.,* (2022) synthesized AgNPs using the aqueous extract of *Areca catechu* L. nut and observed that the synthesized AgNPs are able to scavenge the ABTS radical in a dose dependent manner. They reported that the phytochemicals like flavonoids, phenolics present in the plant extract not only acts as a capping agent but also involved in the scavenging of free radicals. In line with our study, Devi *et al*., (2021) synthesized silver nanoparticles from aqueous extract of *Luffa acutangula* leaf and found that the synthesized silver nanoparticles were able to scavenge ABTS radical much better than the extract. Yücel *et al.,* (2017) encapsulated rosmarinic acid, a phenolic compound into the liposomes and found that the antioxidant activity increases after encapsulation. This is because the encapsulation of rosmarinic acid into the liposomes improved its solubility.

In accordance with the above cited literatures, the ABTS radical scavenging ability of the plant extract and AgNPs is due to the availability of various phytochemicals like phenols, flavonoids and also their role as capping agent. The silver nanoparticles loaded liposomes effectively scavenged the ABTS radical since the solubility of AgNPs are improved after encapsulating them into the liposomes.

4.3.3. Hydroxyl Radical Scavenging Assay

Hydroxyl radicals are produced by Fenton reaction and are the causative free radicals for severe damage to the cells. They even create damage to the cells and the biomolecules that are present adjacent to them. Since hydroxyl radical is highly reactive, it has to be scavenged effectively (Al-Mamary and Moussa, 2021). The hydroxyl radicals in higher concentration can even oxidizes thiol groups in the molecules thereby denatures the major enzymes in our body. Since hydroxyl radicals cause much deleterious effect to the human body, the samples which are having the ability to scavenge these radicals are considered to be potent radical scavengers and also expected to exert same action *in vivo* (Beatrice *et al.,* 2020)

In the present study, the hydroethanolic extract, silver nanoparticles and silver nanoparticles loaded liposomes are allowed to scavenge hydroxyl radicals. All the samples tested exerted a good scavenging potential against hydroxyl radical when the concentration increases. The silver nanoparticles loaded liposomes (IC 50: 152.65 µg/ml) were found to scavenge hydroxyl radicals to a greater extent followed by silver nanoparticles (IC 50: 264.083µg/ml) and hydro Ethanolic extract (IC 50: 334.074µg/ml). From the graph, it was found that the all the samples tested were much effective against hydroxyl radicals and is comparable with quercetin standard.

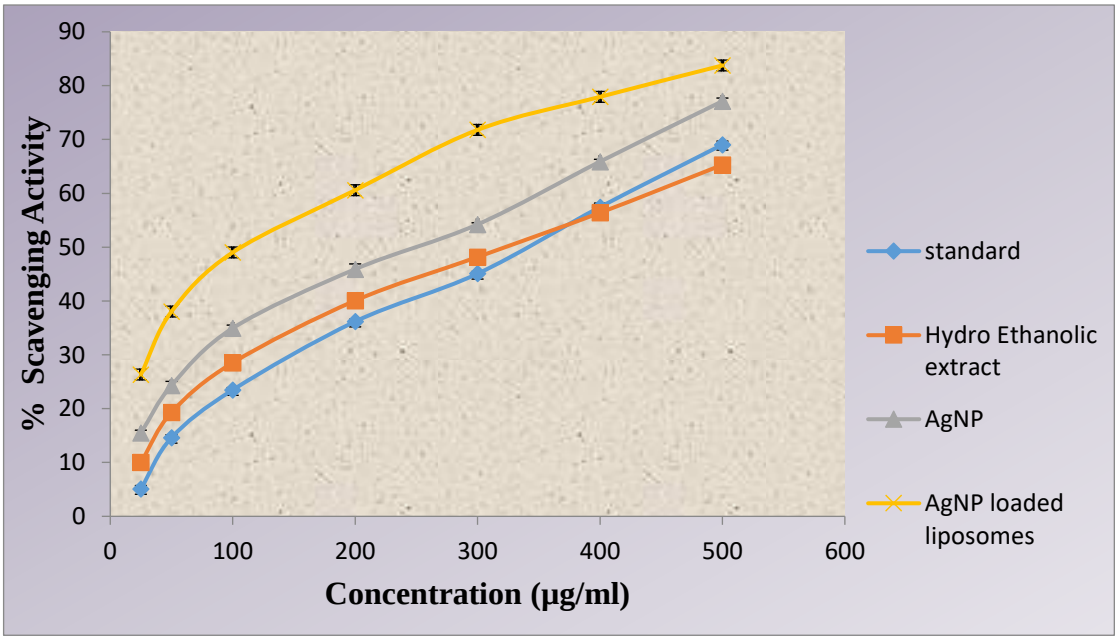

The values are represented as ±SD for triplicates in each category, P< 0.05

Fig. 34: Hydroxyl Radical Scavenging Assay

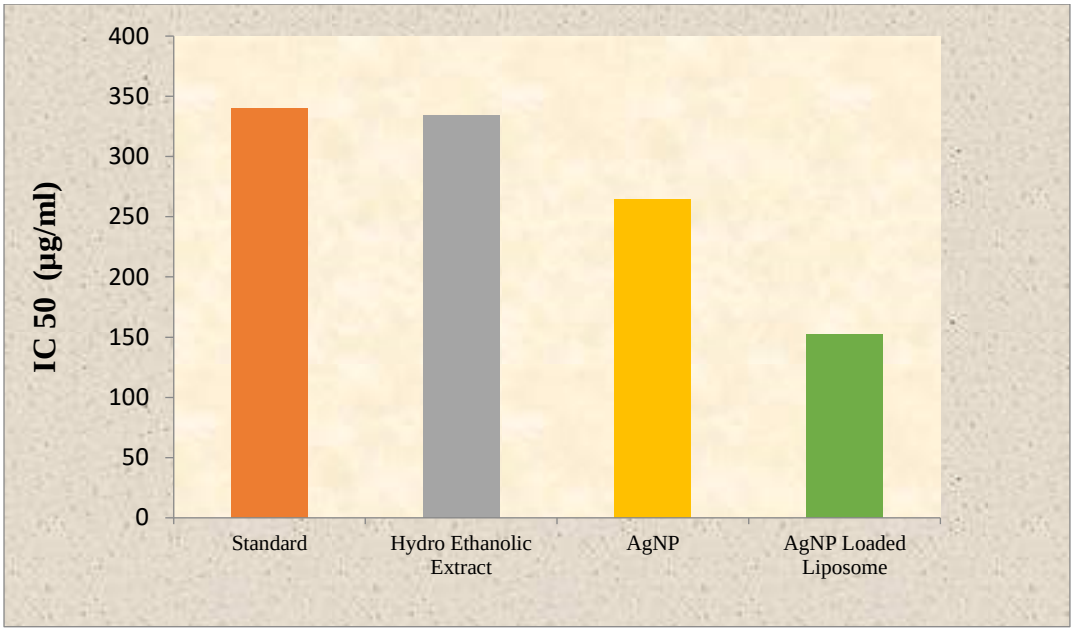

Fig. 35: IC 50 values for Hydroxyl Radical Scavenging Assay

Our results are in correspondence with the several researchers. In accordance with our study, Mo *et al.*, (2021) analysed the hydroxyl radical scavenging potential of *Ailanthus altissima* Swingle and found that the extracts scavenged the hydroxyl radical in a concentration dependent manner. This probable antioxidant property might be due to the tendency of the antioxidants to provide hydrogen to the free radical thereby terminating the free radical chain. In a study carried out by Lalhminghlui and Ganesh (2018), various extracts of *S. wallichii* were analysed for the hydroxyl radical scavenging activity and observed that the ethanolic extracts were found to possess high antioxidant mechanism. This might be probably due to the availability of phenolic compounds in the plant extract. Arumugam *et al.*, (2017) synthesized AgNPs using *Lippia nodiflora* and analysed hydroxyl radical scavenging ability. From their results it was concluded that the synthesized silver nanoparticles were able to scavenge hydroxyl radicals in a concentration dependent manner. This could be due to the inhibition of lipid peroxidation by the synthesized silver nanoparticles. Green synthesized AgNPs from the *C. halicacabum* leaf extract showed a dose dependent scavenging potential against hydroxyl radicals. The phenolic compounds present in the plant extract that acted as a capping agent might be the reason behind scavenging (Sundararajan *et al.*, 2016). Zhijuan *et al.*, 2020 prepared a flavonoid loaded nanoemulsion and observed that the nanoemulsion exhibited highest hydroxyl radical scavenging activity in a dose dependent manner.

In agreement with the above literature, the presence of various phytochemicals like phenols in the tested samples and their ability to donate electrons to the free radicals and also the inhibition of lipid peroxidation increased their hydroxyl radical scavenging potential.

4.3.4. Hydrogen Peroxide Radical Scavenging Assay

Hydrogen peroxide is the major source for hydroxyl radicals that is formed by Fenton's reaction that leads to DNA damage. It can easily cross the cell membrane. The route of hydrogen peroxide exposure to the human body is through inhalation of mist or vapor through eye or skin. On exposure, it readily decomposes to water and oxygen finally leading to the formation of more toxic hydroxyl radical. The prolonged exposure to hydrogen peroxide leads to neurological disorders, tumor and aging (Azhari *et al.*, 2021; Atere *et al.*, 2018).

In the present study, the various samples were subjected to oxidative stress by the addition of hydrogen peroxide under *in vitro.* Among the various samples tested, the silver nanoparticles (IC50: 257.11µg/ml) and silver nanoparticles loaded liposomes (IC50: 236.94µg/ml) of *Tabebuia pallida* were able to scavenge the hydrogen peroxide radical to a greater extent. The hydrogen peroxide radical scavenging ability of both silver nanoparticles and silver nanoparticles loaded liposomes of *Tabebuia pallida* are comparable with that of the standard quercetin (IC50: 341.8µg/ml). However, there is a consistent increase in scavenging potential with increase in concentration was observed.

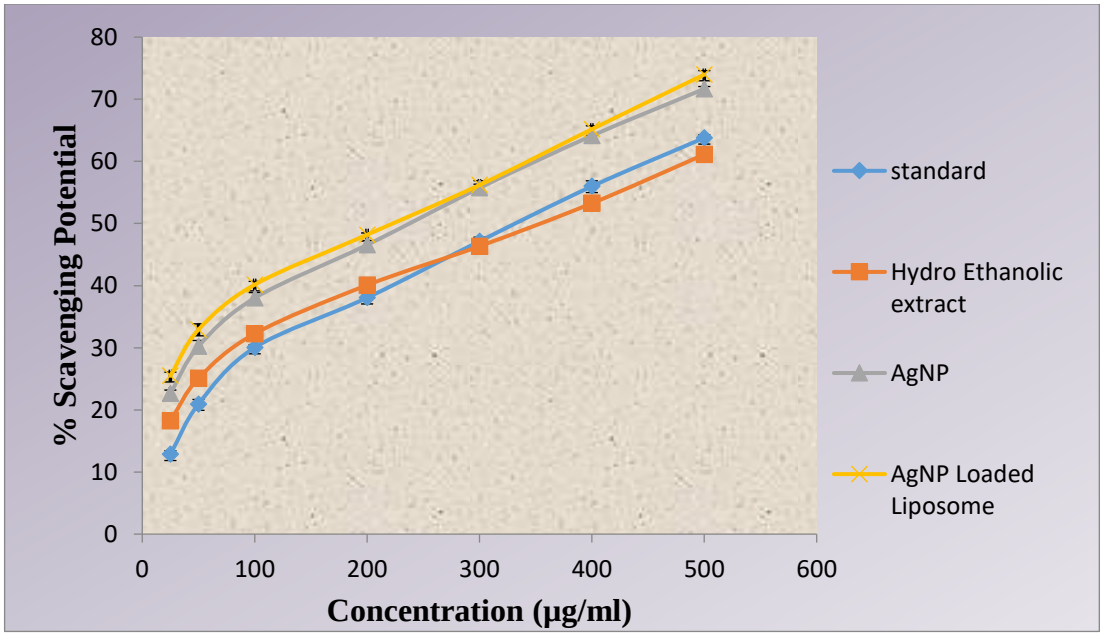

The values are represented as ±SD for triplicates in each category, P< 0.05

Fig. 36: Hydrogen Peroxide Radical Scavenging Assay

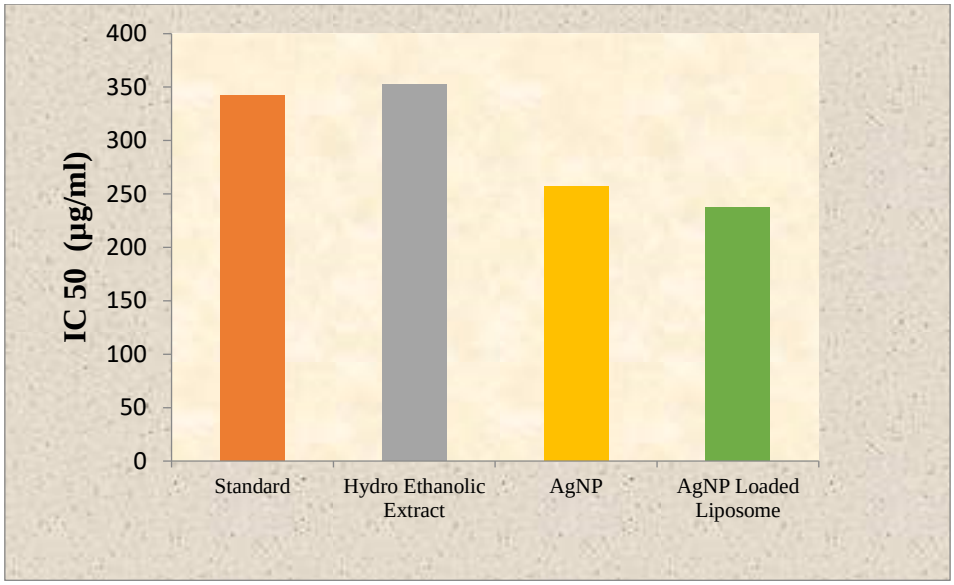

Fig. 37: IC 50 values for Hydrogen Peroxide Radical Scavenging Assay

In accordance with our findings, Sharifi *et al.*, (2018) tested the hydrogen peroxide radical scavenging potential of the *V. persica* extract and observed that the scavenging potential increases when the concentration of the sample is increased and also the *V. persica* extract can scavenge the hydrogen peroxide radical to a greater extent when compared to the standard ascorbic acid. This could be achieved due to the presence of high polyphenol content in the plant extract. Venkanna *et al.*, (2017) prepared various extracts of *Albizia odoratissima* and found that all the extracts tested were scavenged the hydrogen peroxide radical in a concentration dependent fashion. The hydrogen peroxide scavenging ability of these extracts is probably due to the increased concentration of the polyphenols. In a study carried out by Kumar *et al.*, (2021), the green synthesized silver nanoparticles from *C. roseus* extract was found to exert high hydrogen peroxide radical scavenging potential when compared to the *C. roseus* extract. Guntur *et al.*, (2018) synthesized AgNPs using the leaf extract of *Desmostachya bipinnata* and observed that the synthesized silver nanoparticles were able to effectively scavenge the hydrogen peroxide radicals due to the various phytoconstituents or secondary metabolites that played a prominent role in the reduction of silver like terpenoids, and phenolic compounds.

In accordance with the above cited literatures and the findings of the present study, the hydrogen peroxide radical scavenging activity was mainly due to the presence of various

phytoconstituents like polyphenols, terpenoids and phenolic compounds present in the Hydroethanolic extract of *Tabebuia pallida.*

Reducing Power Assay

The ferric reducing power of an antioxidant could be measured by its ability to convert Fe^{3+} to Fe^{2+}. The reducing power was found to increase with increase in absorbance of the sample. The antioxidants present in the sample reduces Fe^{3+} to Fe^{2+} which chelates with potassium ferricyanide present in the solution and turns to blue colour complex which is measured at 700nm *(*Liu *et al.,* 2021; Kiani *et al.,* 2021).

In our study, the hydroethanolic extract, silver nanoparticles and silver nanoparticles loaded liposomes were tested for their ferric ion reducing ability. All the samples tested were able to reduce Fe^{3+} to Fe^{2+} in a dose dependent manner. Among the tested samples the silver nanoparticles loaded liposomes were able to produce high reducing power followed by silver nanoparticles and hydroethanolic extract. The standard quercetin was also found to possess high reducing ability.

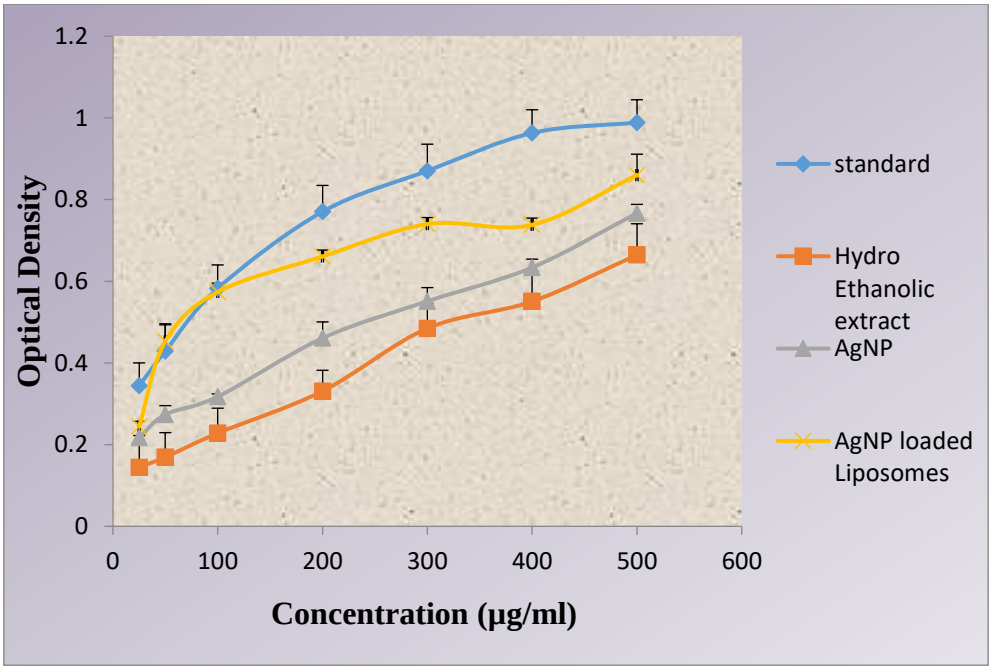

The values are represented as ±SD for triplicates in each category, P< 0.05

Fig. 38: Reducing Power Assay

Abdul *et al*., (2022) tested the ferric reducing ability of *B. acmella* and observed that the extract possesses a significant antioxidant potential. This is due to the electron contributing ability of the antioxidants present in the plant extract. Jasmin *et al*., (2022) prepared various solvent extracts of bark of *Dillenia indica* L., and observed that there is a dose dependent

reducing ability of the extracts. This could be possibly due the presence of antioxidants like polyphenols and flavonoids in the plant extract. In par with our findings, Essghaier *et al*., (2022) synthesized AgNPs from aqueous extracts of wild Olive and Pistachio leaves and observed that the synthesized silver nanoparticles were able to exert a high reducing power than the leaf extracts. This is due to the presence of plant phytochemicals that acted as capping agents which involved in the reduction of Ag^{+} to AgNPs. In accordance with our results Purushothaman *et al*., (2022), synthesized AgNPs from *Murraya paniculata* leaf extracts and observed that the synthesized silver nanoparticles are found to be the potent reducing agent than the extract which is due to the presence of secondary metabolites that are capped on the surface of the synthesized nanoparticles.

The findings of the current study indicate that the phytoconstituents like polyphenols and flavonoids present in the plant extract exerted a ferric reducing potential by donating its electrons. The silver nanoparticles are also found to possess good reducing potential due to the presence of various phytoconstituents in the surface of it. The liposomal encapsulated silver nanoparticles also exhibited good reducing ability which clearly indicates that the encapsulation doesn't affect the antioxidant potential of the silver nanoparticles.

4.3.5. Nitric Oxide Radical Scavenging Assay

Nitric oxide is one of the most predominant biological molecules which is found to possess various physiological effects such as signal transduction, antitumoral and antimicrobial activity and also controls the blood pressure. It also possesses some toxic properties like severe cellular damage as it reacts with oxygen and super oxide radicals. So the surplus NO_2 should be scavenged for the maintenance of healthy homeostasis. The sodium nitroprusside facilitates the formation of nitric oxide which then reacts with oxygen to form nitrite. Thus formed nitrite reacts with naphthyl ethylenediamine and produces a pink colored product which was measured spectrophotometrically at 546nm. The antioxidants present in the extracts donates proton to the nitrite radical which leads to a decrease in the absorbance which reveals the extent of nitric oxide radical scavenging (Singh *et al.,* 2012).

The nitric oxide scavenging potential of hydroethanolic extract, silver nanoparticles and silver nanoparticles loaded liposomes of *Tabebuia pallida* were assayed by using quercetin as the standard compound. All the samples tested were able to scavenge the nitric oxide in a concentration dependent manner and found to possess high scavenging potential and are on par

with the standard quercetin. The scavenging potential observed in the following order silver nanoparticles loaded liposomes > silver nanoparticles > hydroethanolic extract > quercetin with the following IC 50 values: silver nanoparticles loaded liposomes (162.17 µg/ml), silver nanoparticles (184.47 µg/ml), hydro Ethanolic extract (241.73 µg/ml), and quercetin (299.23 µg/ml).

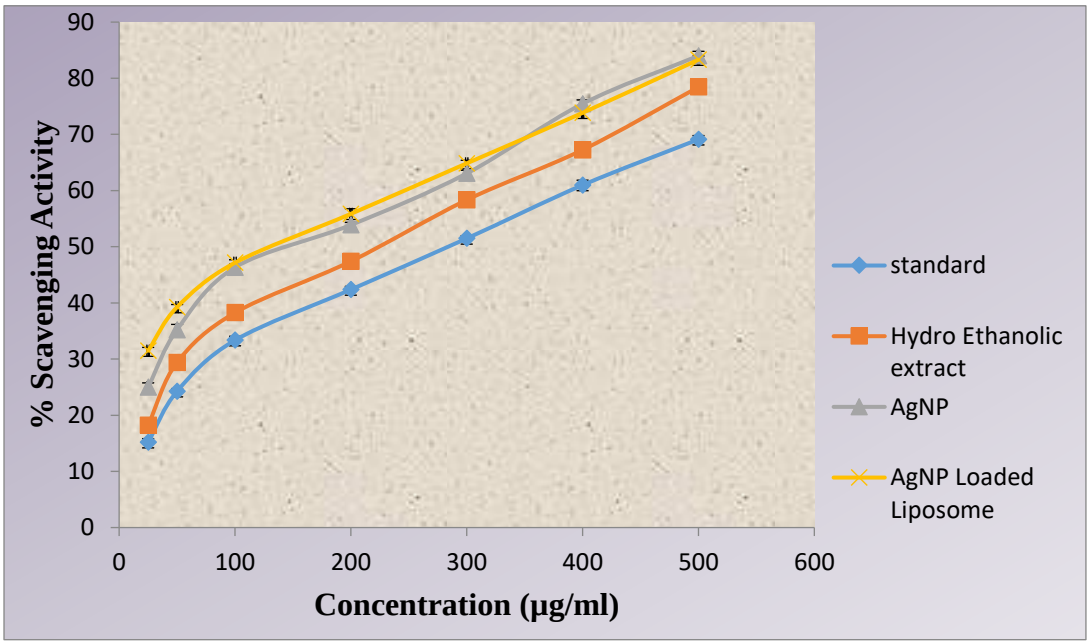

The values are represented as ±SD for triplicates in each category, P< 0.05

Fig. 39: Nitric Oxide Radical Scavenging Assay

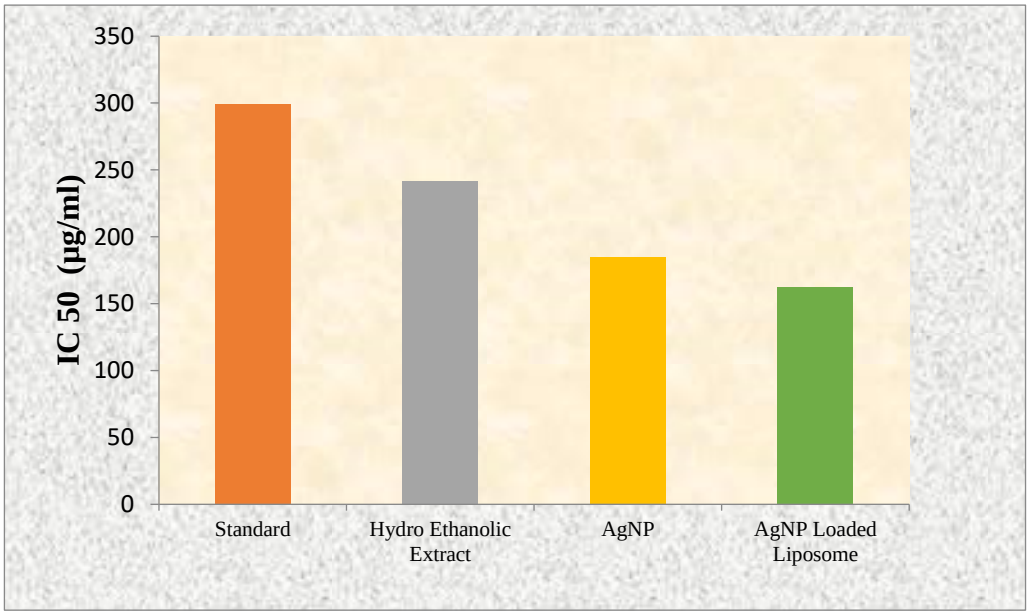

Fig. 40: IC 50 values for Hydrogen Peroxide Radical Scavenging Assay

Fadzai *et al.,* (2014) tested the nitric oxide radical scavenging ability of *C. platypetalum, C. zeyheri,* and *P. curatellifolia* leaf extracts and observed that the scavenging potential is dose dependent. The presence of polyphenol compounds in the extract is responsible for the effective scavenging of nitric oxide radicals. A report published by Preethamol and Thoppil, (2020), prepared the whole plant extract of *Ophiorrhiza pectinata* and carried out nitric oxide radical scavenging assay. They observed that there is a dose dependent nitric oxide scavenging potential of the plant extracts. Adebayo *et al.,* (2021) synthesized AgNPs from *Opuntia ficusindica* extract and observed that the scavenging potential is dependent on the concentration of the sample and the results reveal that the nitric oxide radical scavenging ability of the synthesized silver nanoparticles were found to be higher than the plant extract. This high scavenging potential might be due to the involvement of various phytoconstituents that played a role as reducing agent for the formation of AgNPs. The present results are in concurrence with the previous study carried out by Yugal *et al.,* (2022) who synthesized AgNPs from *Gracilaria edulis* and carried out nitric oxide radical scavenging assay and observed that the synthesized silver nanoparticles were able to exert a dose dependent scavenging potential and also the NO_2 radical scavenging ability was higher for the silver nanoparticles than the plant extract. This is due to the fact that the silver and the phytoconstituents available in the plant extract and that is present in the AgNPs as reducing agent was also involved in the scavenging activity.

The tested samples were able to scavenge the nitric oxide radicals effectively due to the presence of polyphenol compounds in the plant extracts and also the phytoconstituents that are present in the surface of the synthesized silver nanoparticles played a major role in scavenging the nitric oxide radicals.

Thus the results of Phase III clearly show that the silver nanoparticles of *Tabebuia pallida* and silver nanoparticles loaded liposomes could readily scavenge the team of radicals (DPPH, ABTS, Hydrogen peroxide, Hydroxyl and Nitric oxide) tested in the present study indicating their potential to act as a good antioxidant and radical quencher. Further it becomes necessary to assess the anticancer efficacy of the silver nanoparticles and silver nanoparticles loaded liposomes of *Tabebuia pallida* to validate the results obtained in phase III.

Phase IV

4.4. Evaluation of Anticancer potential of AgNPs of *T. pallida* leaves and their Nanoliposomes

4.4.1. MTT Dye Reduction Assay

MTT is a tetrazolium dye that contains quaternary tetrazole which is a positively charged ring structure that contains four nitrogen surrounded by three aromatic rings that contains one thiazolyl ring and two phenyl moieties. A violet colored formazan molecule that is insoluble in water is formed when the MTT dye is reduced by disrupting its tetrazole ring. Since MTT is positively charged, it can easily penetrate the cell membrane and also the inner mitochondrial membrane of live cells and is reduced to the formazan product. This assay is mainly used to analyze the metabolic activity of the cells.

MTT assay was carried out to determine the cytotoxic effect of the hydroethanolic extract, silver nanoparticles and silver nanoparticles loaded liposomes of *Tabebuia pallida*, with different concentrations of the samples (20, 40, 60, 80 and 100 µg/ml). Fig. 41 shows that the cells alone were considered as control and the viability of the control group cells was fixed to be 100. The findings of the current study reveals that all the treatment groups exhibited dose dependent cytotoxic potential against Molt-3 cells. Among the various treatment groups tested, the silver nanoparticles loaded liposomes was found to possess high cytotoxic effect with an IC50 value of 41.75 µg/ml, followed by silver nanoparticles (IC50=79.25 µg/ml) and the hydroethanolic extract (IC50 =100 µg/ml) against Molt-3 cells. From this observation, it could be concluded that all the treatment groups exhibited a significant cytotoxic effect against Molt-3 cells.

To determine whether these treatment groups affects the normal cells, MTT assay was carried out to test the cytotoxic effects of various treatment groups against Peripheral Blood Lymphocytes (Fig. 42) which is the normal counterpart of the Molt-3 cells. The results revealed that all the treatment groups exhibited a very less or minimal cytotoxicity to the normal cells. The IC50 values of the cytotoxicity against PBL was given as follows: hydroethanolic extract: 129.24 µg/ml, silver nanoparticles: 156.73 µg/ml and silver nanoparticles loaded liposomes: 169.47 µg/ml. From this, it is evident that the various treatment groups exhibited a very less or minimal cytotoxicity to the normal PBL since the IC50 values were high. The cytotoxicity of the treatment groups against PBL was in the following order hydroethanolic extract > silver

nanoparticles > silver nanoparticles loaded liposomes. From this, it is evident that the silver nanoparticles and silver nanoparticles loaded liposomes exerted a targeted drug delivery which caused toxicity only to the Molt-3 cells and does not cause cytotoxicity to the peripheral blood lymphocytes much.

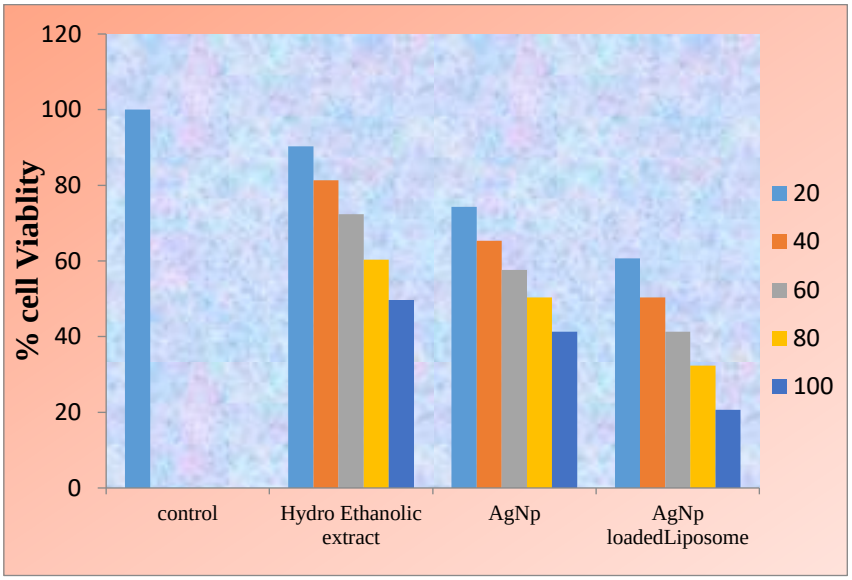

The values are represented as ±SD for triplicates in each category, P< 0.05

Fig. 41: MTT Dye Reduction Assay (Molt-3)

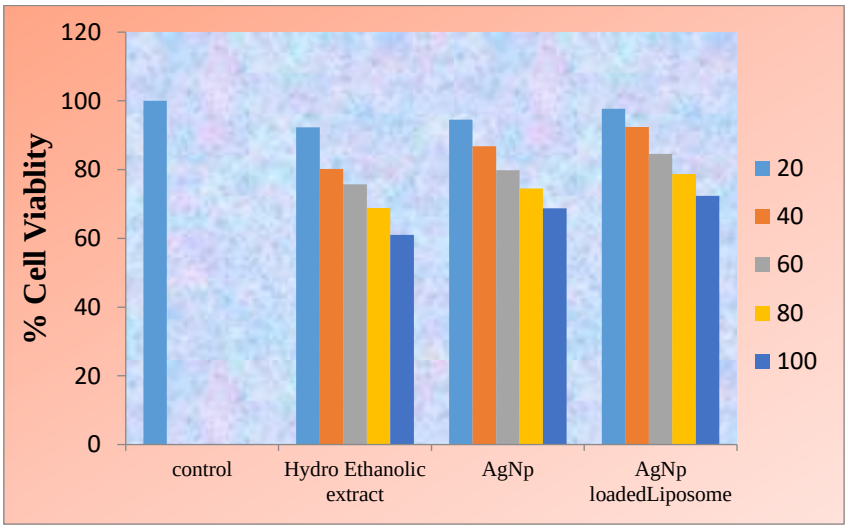

The values are represented as ±SD for triplicates in each category, P< 0.05

Fig. 42: MTT Dye Reduction Assay (PBL)

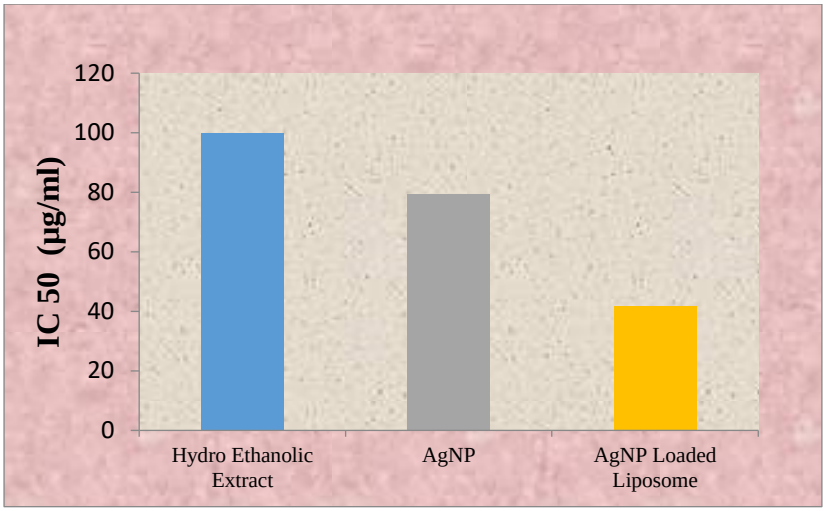

Fig. 43: IC 50 values for MTT Dye Reduction Assay (Molt-3)

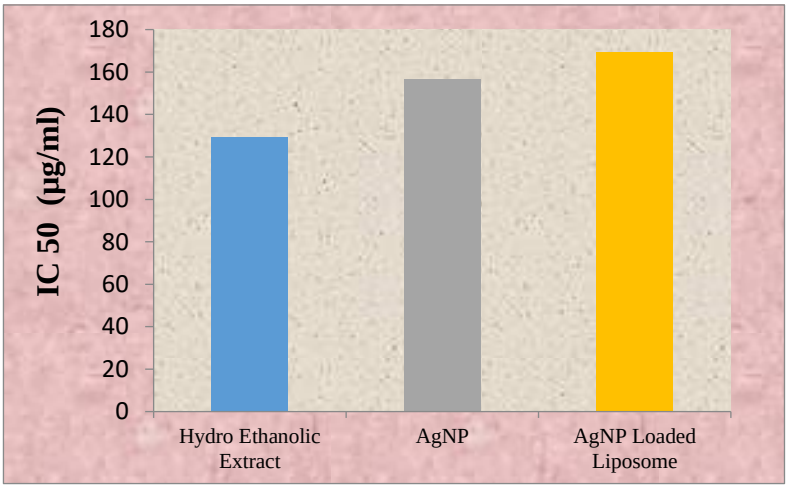

Fig. 44: IC 50 values for MTT Dye Reduction Assay (PBL)

In line with our study Niksic *et al.*, (2021) extracted essential oil from *Thymus vulgaris* L. and carried out MTT dye reduction assay against three different cell lines (MOLT-4, H460 and MCF-7). They observed that the cytotoxic activity of the essential oil was concentration dependent. Among the various cell lines subjected to analysis the essential oil can exert high cytotoxic effect to MCF-7 cells followed by MOLT-4 and H460 cell line. This is due to the presence of various phytochemicals that are present in the essential oils. Hawary *et al.*, (2021) carried out cytotoxic effect of five *Tabebuia* species against three different cancer cells CACO2, MCF-7, and HepG2. Among the tested species of *Tabebuia*, *T. rosea* stem extract was found to be potent against HepG2 cell line, stem extract of *T. pulcherrima* was found to cause high cytotoxicity to CACO2 cell line and *T. pallida* L. stem extract being highly toxic to MCF-7 cell line. This good cytotoxic effect is because the *Tabebuia* species were found

to contain alkaloid, naphthoquinones, particularly β-lapachone, which might play a possible role in cell death via apoptosis.

Karimi *et al.,* (2020) synthesized AgNPs using *Achillea millefolium* extract and carried out MTT dye reduction assay against Molt-4 cell line and observed that the viability of the cells decreases with increase in concentration of the AgNPs. This is due to the combinatorial effect of green synthesized silver nanoparticles and the secondary metabolites present in the *Achillea millefolium* extract. The silver nanoparticles might interact with phosphate groups and nitrogen bases present in DNA and also with the functional groups of proteins thereby induces significant cytotoxic potential. The electrostatic interaction between the cancer cells and the silver nanoparticles might also pave the way for its cytotoxic potential. Ikram *et al.,* (2020) carried out green synthesis of AgNPs using *Fagonia indica* extract and observed a dose dependent inhibition of breast cancer cells growth. The possible mechanism behind this cytotoxic effect is that nanoparticles induces the cancer cells membrane permeability and induces the activation of caspases and also generates ROS.

Hee *et al.,* (2019) prepared dual drug (metformin and sodium salicylate) loaded liposomes and carried out MTT dye reduction assay against MCF-7 breast cancer cells. The results revealed that the double drug loaded liposomes was potent enough to exert highest cytotoxic potential against MCF-7 when compared to the single drug loaded liposomes and single and dual free drugs. This highest cytotoxic effect is due to the fact that the liposomes enhances the permeability of the drugs through MCF-7 cells and accumulate into the cancer cells which facilitates the targeted action of the drug, thereby reduces side effects. Zarrabi *et al.,* (2021), prepared Curcumin loaded liposomes and stealth liposomes and evaluated the cytotoxicity using MTT dye reduction assay against normal cells (L929) and cancer cells (MCF7). From the results, it was found that both curcumin loaded liposomes and stealth liposomes does not cause significant cytotoxicity to the normal cells while free drug showed a significant cytotoxic effect. Stealth liposomes were found to be highly effective against MCF 7 cells, which clearly indicate the targeted drug delivery nature of the liposomes.

From the above cited literatures and the findings of the present study, it could be considered that the silver nanoparticles and silver nanoparticles loaded liposomes of *Tabebuia pallida* exerted targeted drug delivery to Molt-3 cells without harming the PBL much.

4.4.2. SRB Assay

SRB assay is mainly used to analyse the cytotoxic effect of the cells. It is highly preferable by the researchers, since it is cost effective. It is more or less similar to the other cytotoxicity assay like MMT or colonogenic assays. The major principle of SRB assay is the ability of the sulphorhodamine B dye to bind with the cells that are fixed by trichloroacetic acid. It is sensitive and appropriate assay for cytotoxicity induced by various drugs.

The results of the current study reveals that all the three treatement groups exhibited a significant toxicity to the Molt-3 cells. The cytotoxicity was found to be dose dependent. It was evident from the graph that the cytotoxicity was in the following order: Hydroethanolic extract < silver nanoparticles < silver nanoparticles loaded liposomes. Among the treatment groups, the silver nanoparticles loaded liposomes was found to be highly effective against Molt-3 cells with an IC 50 value of 38.63 µg/ml. On the other hand, when the peripheral blood lymphocytes were treated with various treatment groups a minimal cytotoxicity was observed. When compared to the various treatment groups the silver nanoparticles loaded liposomes was found to exert very minimal cytotoxicity to the PBL cells. This clearly indicates the targeting ability of the liposomal encapsulated silver nanoparticles, while sparing the normal PBL.

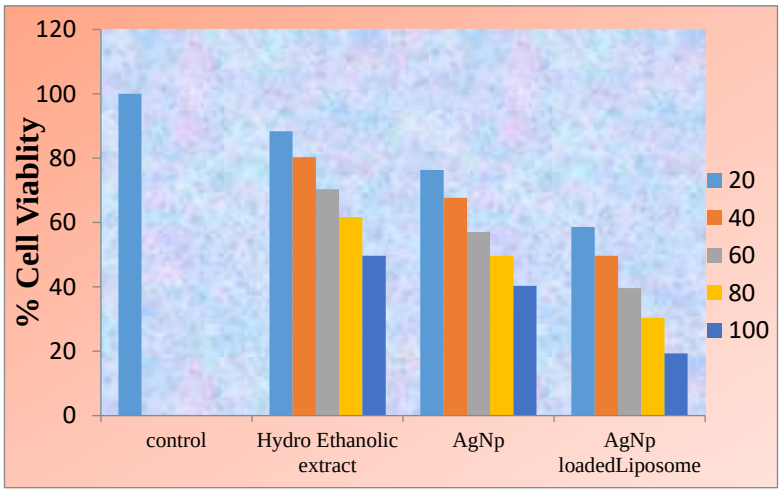

The values are represented as ±SD for triplicates in each category, P< 0.05

Fig. 45: SRB Assay (Molt-3)

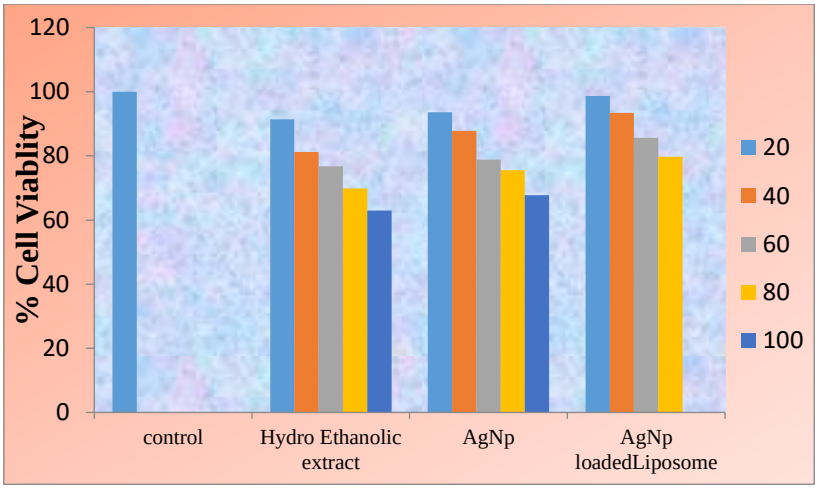

The values are represented as ±SD for triplicates in each category, P< 0.05

Fig. 46: SRB Assay (PBL)

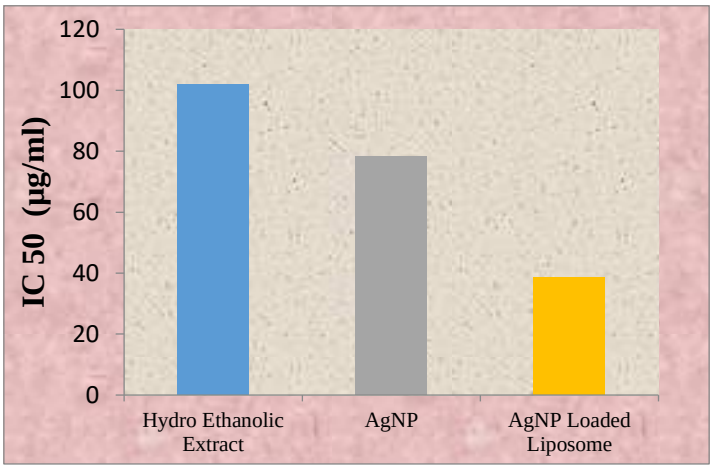

Fig. 47: IC 50 values for SRB Assay (Molt-3)

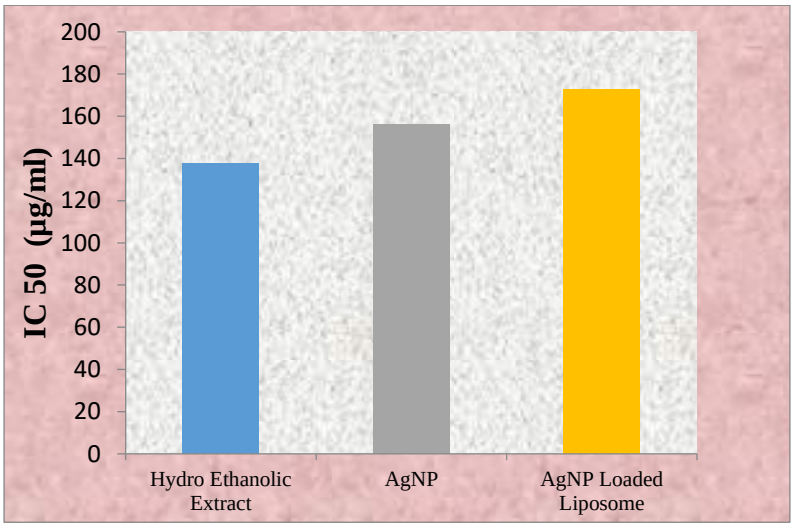

Fig. 48: IC 50 values for SRB Assay (PBL)

In agreement with our findings, Qanash *et al.,* (2022) prepared *D. caffra* extract and analysed for its cytotoxicity against HepG2 cells and observed that the extract exhibited a dose dependent cytotoxicity. It was found to exert only a minimal toxicity at lower concentration and when the concentration was increased the percentage of the viable cells was found to be decreased. Albinhassan *et al.,* (2021) prepared *Avicennia marina* leaf extracts using various solvents and analysed its cytotoxic ability against three cell lines HCT-116, MCF-7, and HepG2 using SRB assay. Among the various extracts tested and hexane extract was found to render a high cytotoxicity against HCT-116 cell line. This cytotoxicity was achieved by the activation of pro apoptotic and apoptotic factors by the plant extract. In line with our study, Mohamed *et al.,* (2022) synthesized silver nanoparticles from polysaccharides of *Leucaena leucocephala* seeds and carried out cytotoxicity assay against HEPG-2, HCT-116, and MCF-7 cell lines. The silver nanoparticles are found to exert high cytotoxic effect against all the tested cell lines and the cytotoxicity was found to be in par with the standard drug used for the analysis. This high cytotoxicity is obtained because of the smaller size of the nanoparticle and the capping agent that is present in the surface of the nanoparticle which exerted an antitumor potential. Shejawal *et al.,* (2021) synthesized AgNPs from lycopene extract of tomato and carried out SRB assay to evaluate the cytotoxic effect of the synthesized AgNPs and reported that the silver nanoparticles are very effective in causing cytotoxicity against COLO320DM cell line. Kong *et al.,* (2022) prepared Epirubicin and Resveratrol loaded liposomes and analysed its cytotoxic activity and found that the liposomal loaded formulations are much effective against C6 glioma cells when compared to the unloaded or free Epirubicin and Resveratrol. This is due to the fact that the liposomes posess high cellular uptake which leads to its high cytotoxicity.

Thus, in the current study the Hydroethanolic extract, silver nanoparticle and silver nanoparticles loaded liposomes of *Tabebuia pallida* are found to be effective in causing cytotoxicity to the Molt-3 cells. This might probably due to the availabilty of various phytoconstituents in the plant extract which also played a significant role in reducing silver nitrate. Since the size of the silver nanoparticles is very small, the uptake of it by the cells is high which leads to more cytotoxicity. The silver nanoparticles loaded liposomes are found to be the best among the treatment groups since the liposomes enhanced the cellular permeability thus leading to high cellular toxicity. All the treatment groups don’t exhibit considerable cytotoxic effect to the normal counterpart PBL which clearly specifies the targeting nature of the treatment groups.

Measurement of Apoptosis- Annexin V/FITC staining

Annexin V/FITC staining is mainly applied for determining cell death via apoptosis. Annexin V can bind strongly with a membrane phospholipid, phosphatidyl serine which is relocated from inner side of the membrane to the outer side of the membrane. The Propidium iodide can bind with DNA and it has the ability to enter into late apoptotic and necrotic cells.

The Hydroethanolic extract, silver nanoparticles and silver nanoparticles loaded liposomes of *Tabebuia pallida* were treated with Molt-3 cells and subjected to measurement of apoptosis by Annexin V FITC staining. From the results, it was observed that in the case of control, most of the cells are in live phase, and when the cells are treated with various treatment groups of *Tabebuia pallida* the cells were found to be distributed in both early and late apoptotic phase. When the cells are treated with hydroethanolic extract 61.85% cells are in early apoptotic phase, in the case of silver nanoparticles treated, 86.41% cells are in early apoptotic phase and in the group treated with silver nanoparticles loaded liposomes 46.62% of the cells are in early apoptotic phase and 51.82% of the cells are in late apoptotic phase and also only 0.01 % of the cells are found to be in live phase. This clearly indicates the apoptosis inducing ability of the silver nanoparticles and silver nanoparticles loaded liposomes is very rapid. On the other hand, when the PBL cells are treated with various treatment groups, the percentage of apoptotic cells are very less compared to the Molt-3 cells treated groups. When the Hydroethanolic extract is treated with PBL cells 78.36% of the cells are in live phase and 21.60% of the cells are in early apoptotic phase. In the case of silver nanoparticles treated PBL, 90.57% of the cells are in live phase, 1.63% of the cells are in early apoptotic phase and 6.20% of the cells are in late apoptotic phase. When the PBL cells are treated with silver nanoparticles loaded liposomes 93.36% of the cells are in live phase and 6.46% of the cells are in early apoptotic cells. This clearly indicates that the silver nanoparticles loaded liposomes doesn't cause cytotoxicity to the normal PBL cells but it is highly effective against the Molt-3 leukaemic cells. This proves the targeted drug delivery nature of the liposomes and also the apoptosis inducing ability of the silver nanoparticles of *Tabebuia pallida* loaded liposomes is high as reflected by the presence of late apoptotic cells.

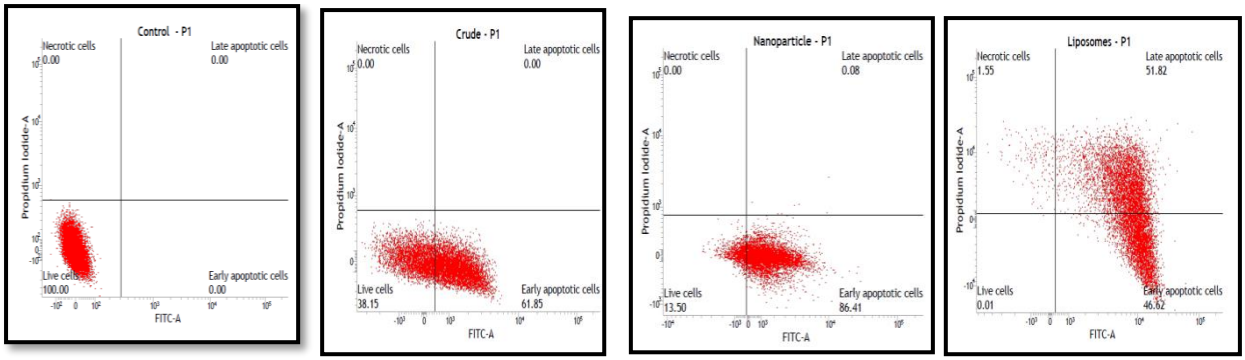

Control (cells alone) hydroethanolic extract silver nanoparticles silver nanoparticles loaded lipsomes

Fig. 49: Measurement of Apoptosis- Annexin V/FITC staining (Molt-3 cells)

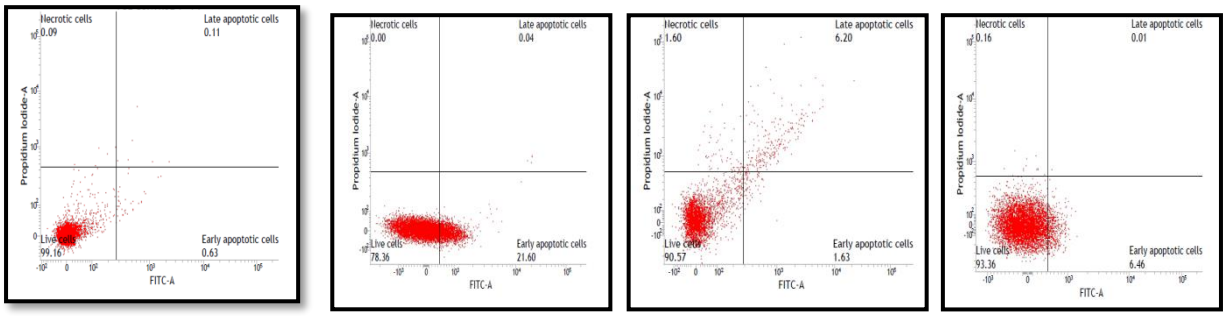

Control (cells alone) hydroethanolic extrac silver nanoparticles silver nanoparticles loaded lipsomes

Fig. 50: Measurement of Apoptosis- Annexin V/FITC staining (PBL cells)

In accordance with our findings, Al-Zharani *et al*., (2021) prepared Hydroethanolic extract of *Datura innoxia* and detected the apoptosis against LoVo colon cancer cells using Annexin V/FITC staining and observed that the cells are in live phase in the case of control, when the cells are treated with the extract, more number of cells are found to be in early apoptotic phase and when the concentration of the extract is increased, the cells were found to be present in both early and late apoptotic phase. This clearly indicates that the *Datura innoxia* extract treatment activated the apoptosis signaling molecules. Richard *et al*., (2022) prepared Root Extract of *Prunus Africana* and observed that there is a dose dependent apoptosis inducing ability of the prepared extracts against human prostate cancer. This is due to some of the bioactive compounds that are present in the root extract. Xu *et al*., (2020) synthesized silver nanoparticles from aqueous extracts of *Ginkgo Biloba* and carried out Annexin V/FITC staining against cervical cancer cells and observed that the apoptosis inducing ability of the synthesized AgNPs increases with increase in concentration. This clearly indicates that the synthesized silver nanoparticles triggered the activation of apoptosis inducing molecules. In a

study carried out by Noorbazargan *et al*., (2021), the green synthesized silver nanoparticles of *Uniperus chinensis* extract exhibited a dose dependent apoptosis inducing ability against A549 cells. The cells that are treated with the extract are found to be present in high concentration in late apoptotic and necrotic phase when compared to the control cells. Alrumaihi *et al.*, (2022), prepared Diallyl disulfide and oxaliplatin loaded liposomes and measured the apoptosis inducing ability against HCT116 and RKO colon cancer cells. The results revealed that the most of the treatment groups induced late apoptosis which clearly indicates the anticancer potential of the synthesized liposomes. This is achieved by the targeted drug delivery of the Diallyl disulfide and oxaliplatin to the cancer cells thereby, preventing undesired adverse effects. Sahand *et al.*, (2022) prepared Nano-liposomal formulation using zein hydrolysate and observed that the liposomes loaded zein hydrolysate was found to induce apoptosis in an effective manner as the cells are distributed both in early and late apoptotic phase when compared to the free zein hydrolysate where the cells are present only in the early apoptotic phase. This might be due to the effective membrane permeability of liposomal loaded zein hydrolysate to the cancer cells.

From the above literatures cited and the results obtained in our study, it could be concluded that the different phytochemicals present in the extract induces the apoptotic genes and the nanosize of the synthesized nanoparticles facilitated the diffusion into the cancer cells thereby exerting an effective apoptotic pattern. The silver nanoparticles loaded liposomes are much effective against Molt-3 cells since the liposomal encapsulation increases the permeability of drug into the cancer cells. On the other hand, the treatment groups did not affect the PBL cells much which clearly indicate the targeted action only against Molt-3 cells, while sparing the normal peripheral blood lymphocytes.

4.4.4. Analysis of Mitochondrial Membrane Potential by JC1 Staining

During apoptosis, major events occurs in the mitochondria of a cell exerts membrane changes. One important change among that is the loss of mitochondrial membrane potential. An electrochemical proton gradient is maintained inside the mitochondria which is useful for the synthesis of ATP. During apoptosis, this mitochondrial membrane potential is lost. So mitochondrial membrane potential is considered as one of the key parameters in measuring apoptosis. JC-1 is a cationic, lipophilic dye that selectively enters into the mitochondria and accumulates into it forming some aggregate complexes called J-aggregates. These J aggregates gets excited at 590 nm and emits red spectrum instead of its original green colour. So when the

cells are healthy with normal mitochondrial membrane potential, the JC-1 dye enters and accumulates inside the mitochondria forming red coloured J-aggregates. On the other hand, when the cells are under apoptosis, there is a loss of mitochondrial membrane potential which retains the green coloured monomers (Sivandzade *et al.*, 2019).

In the present study, the treated and control cells were stained with JC-1 dye for analysing the mitochondrial membrane potential. From the results, it was observed that, after treating Molt-3 cells with hydroethanolic extract, AgNPs and AgNP loaded liposomes, there was a loss of mitochondrial membrane potential to a greater extent was observed which was confirmed by the formation of more green colored monomers and less J-aggregates. Among the treatment groups, silver nanoparticles loaded liposomes were found to exert a high mitochondrial membrane potential disintegrity which is revealed by the formation of more monomers. In the case of Molt-3 control, there are more J-aggregates which indicate its intact mitochondria. On the other hand, when the normal peripheral blood lymphocytes were treated with various treatment groups, there is a more number of J- aggregates, appeared which clearly indicates that the treatment groups don't affect the peripheral blood lymphocytes much. Hence the mitochondrial membrane potential integrity is maintained. This clearly indicates that the various treatment groups are effective only against Molt-3 cells but doesn't create any ill effects to the normal peripheral blood lymphocytes.

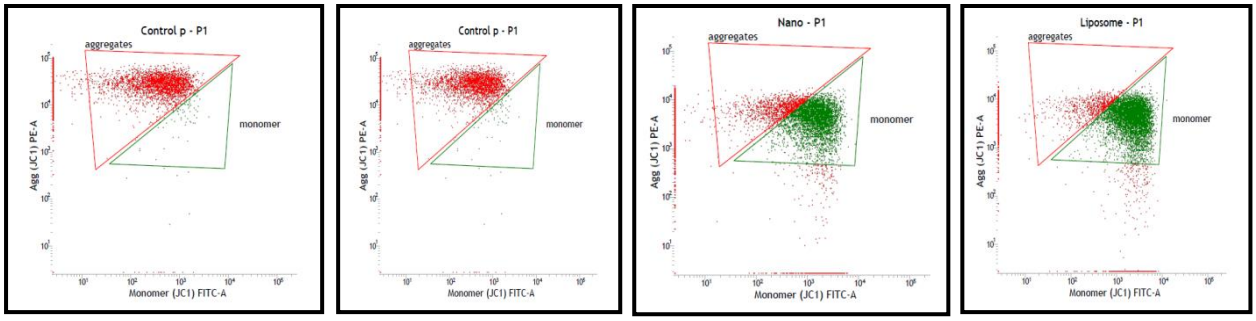

Control(cells alone) hydroethanolic extracts silver nanoparticles silver nanoparticles loaded lipsomes

Fig. 51: Analysis of Mitochondrial Membrane Potential by JC1 Staining (Molt-3 cells)

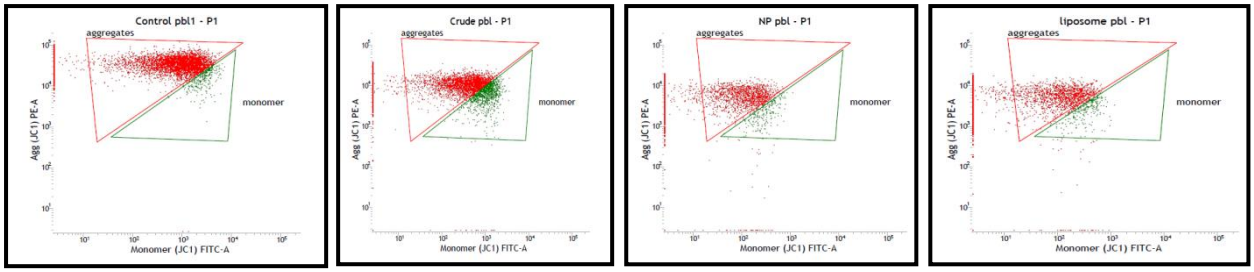

Control (cells alone) hydroethanolic extracts silver nanoparticles silver nanoparticles loaded lipsomes

Fig. 52: Analysis of Mitochondrial Membrane Potential by JC1 Staining (PBL cells)

In agreement with the above findings, Kim *et al.*, (2016) prepared *Torilis japonica* extract and examined its apoptosis inducing ability against HCT116 colorectal cancer cells using JC-1 staining and observed that there is a loss of mitochondrial membrane potential to greater extent when the concentration of the extract is increased. Mansurah *et al.*, (2022), prepared various solvent extracts of *P. bicalyculata* fresh leaves and carried out JC-1 staining to analyze mitochondrial membrane potential in HeLa and MRC5-SV2 cell lines. The results revealed that there is a loss of mitochondrial membrane potential to a greater extent when the cancerous cells are treated with the various solvent extracts of *P. bicalyculata*. The loss of mitochondrial membrane integrity was found to be dependent on both concentration of the treatment groups and also the time of exposure. Jiangyan *et al.*, (2021) analysed the mitochondrial membrane potential of A549 cells after treatment with silver nanoparticles. Thus it was confirmed that the silver nanoparticles treatment collapsed the mitochondrial membrane stability. This might be due to the production of apoptotic and pro apoptotic factors by the silver nanoparticles. Plackal *et al.*, (2018), synthesized silver namnoparticles using *Rubus fairholmianus* leaf extract and measured the mitochondrial destabilization activity and concluded that synthesized silver nanoparticles increased the depolarization of mitochondrial membrane potential thereby leading to apoptosis, but there is no change in polarization of the control cells was observed. Liao *et al.*, prepared Iridium-loaded PEGylated liposomes and carried out mitochondrial membrane potential analysis and observed that both free iridium and PEGylated liposomal loaded iridium exerted a mitochondrial dysfunction or collapse which leads to apoptosis. When compared to the free iridium, PEGylated liposomal loaded iridium was found to be highly effective in causing mitochondrial dysfunction.

From the above cited literatures and the findings of the present study, it is clear that all the treatment groups exerted mitochondrial dysfunction to a greater extent which is due to the activation of apoptotic factors. Among the tested groups liposomal silver nanoparticles of

Tabebuia pallida are found to exert high mitochondrial dysfunction which might probably due to the high membrane permeability of the liposomes, thereby achieving targeted delivery to Molt-3 cells causing apoptotic cell death. However, the AgNPs of *Tabebuia pallida* loaded liposomes did not cause any loss in the mitochondrial membrane potential indicating its non-toxic property in the normal counterpart peripheral blood lymphocytes, which may help in minimizing the adverse effects caused during cancer therapy.

4.4.5. Cell Cycle Analysis

Cell cycle involves a series of modifications which ultimately results in cell division and cell growth. Flow cytometry is used for the analysis of cell cycle at a single cell level. It will analyze the cell cycle based on the measurement of cellular DNA content. Proliferation of cells mainly relies on the cell cycle process, if there is any discrepancy in the cell cycle it leads to various diseases like cancer. The cancer cells are found to possess an abnormal cell cycle. Recently natural compounds or medicinal plants are used as anticancer drugs which usually disrupt the progression of cell cycle thereby preventing abnormal cell proliferation (Anusree and Sonal, 2021).

Cell cycle analysis was carried out to analyze the phase of the cell cycle at which the cells are arrested. In the case of Molt-3 control, the cells were found to be distributed in all the phases of the cell cycle. But when the Molt-3 cells were treated with various treatment groups like Hydroethanolic extract, silver nanoparticles and silver nanoparticles loaded liposomes of Tabebuia pallida, they cell were found to be arrested in G0-G1 phase which is confirmed as the S-phase of the cell cycle having very less number of cell population. On the other hand, when the peripheral blood lymphocytes are treated with various treatment groups, the cells were found to be distributed in all the phases of the cell cycle which indicates that the treatment groups didn't alter the cell cycle phases of peripheral blood lymphocytes.

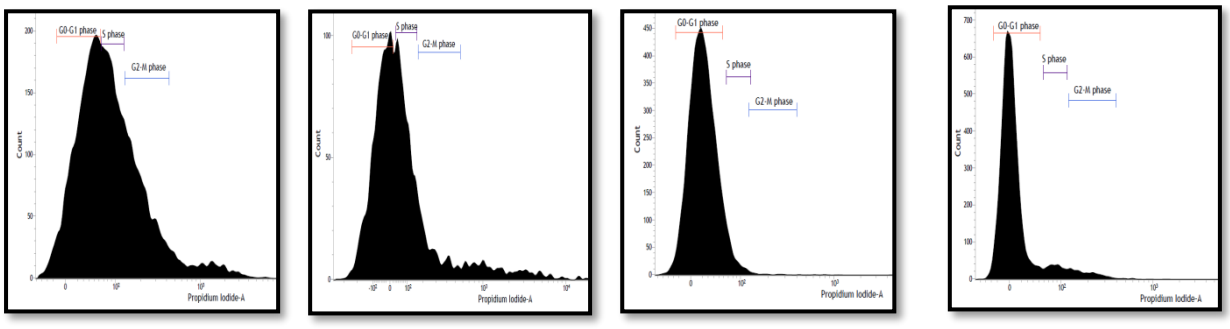

Control | hydroethanolic extract | silver nanoparticles | silver nanoparticles loaded lipsomes

Fig. 53: Cell cycle Analysis (Molt-3 cells)

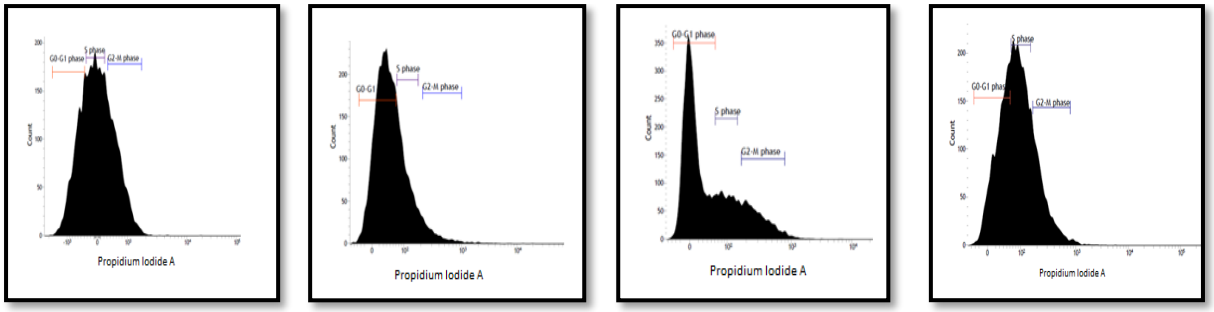

Control | hydroethanolic extract | silver nanoparticles | silver nanoparticles loaded lipsomes

Fig. 54: Cell cycle Analysis (PBL cells)

In agreement with the above results, Barnawi *et al., (*2021) prepared chloroform extract of *Juniperus phoenicea* and carried out cell cycle analysis using flow cytometer. From the results they concluded that the extract treated MCF-7 cells were blocked in G0-G1 phase, whereas in the untreated control, the cells were distributed in all the phases of the cell cycle. The phytoconstituents available in the plant extract might involve in the inhibition the cell cycle at G0-G1 phase. Sultana *et al*., (2022) prepared leaf extracts of *Excoecaria agallocha* L. and analysed its role in arresting cell cycle on SiHa HPV 16+ cell line. From the cell cycle pattern observed the plant extract arrested the cells in G2-M phase of the cell cycle which is evident from the accumulation of more cells in that particular phase and also they tested the cell cycle arresting ability of Cisplatin and observed that after treatment the cells were arrested in G0-G1 phase of the cell cycle. The secondary metabolites present in the plant extract might play a possible role in blocking the cells at various phases of the cell cycle. Saad *et al*., (2018) synthesized AgNPs from aqueous extract of *Nepeta deflersiana* and carried out cell cycle analysis to examine at which phase of the cell cycle the cervical cancer cells were arrested by the AgNPs. The results revealed that the cells were blocked in sub G1 phase which is evident from the highest population of cells accumulated in sub G1 phase. Noorbazargan *et al*., (2021) synthesized silver nanoparticles from *Juniperus chinensis* leaf extracts and analysed for its cell cycle arrest in A549 cells. From the cell cycle pattern, it was observed that the cells were arrested in G0-G1 phase as there is an increase in cell population in that particular phase. Hong *et al*., (2019) prepared ginsenosides loaded liposomes and analysed its anticancer potential against BGC-823 cell line by performing cell cycle analysis and observed that the cells were blocked in G0/G1 phase of the cell cycle. This probably due to the delivery of high concentration of ginsenosides into the tumor site by the liposomes.

Thus the findings of the present study reveals that all the treatment groups were able to exert block the cell cycle in G0-G1 phase which might probably due to the availability of various phytoconstituents in the plant extract and also the smaller size of the synthesized silver nanoparticles entered the cell membrane easily and exhibited cell cycle arrest. The silver nanoparticles loaded liposomes also blocked the cell cycle at G0-G1 phase, which due to the targeting ability of the liposomes and delivering high concentration of the synthesized silver nanoparticles into the tumor cell. On the contrary various treatment groups doesn't harm the normal peripheral blood lymphocytes where the cells were distributed normally in all the phases of the cell cycle proving the non-toxic property of the silver nanoparticles of *Tabebuia pallida* loaded liposomes. Thus the present study results in deriving a conclusion that green synthesized silver nanoparticles of *Tabebuia pallida* mediated by sunlight are spherical, face centred cubic crystalline structure which exerts nanoparticle characteristics. These nanoparticles were further encapsulated using liposomes to increase their stability and make them suitable for drug delivery. These stable nanocarriers with high encapsulation efficiency were then checked for their radical scavenging potential. The results confirm their greater potential for quenching radicals that mediate oxidative stress in dose dependent manner. Further to assess, whether the antioxidants radical scavenging and anticancer property is exerted only in cancer cells due to the targeted delivery by the liposomes. Anticancer efficacy was assessed in Molt-3 cells and PBL. The results indicate that it could exert its anticancer effect due to the presence of phytoconstituents in Molt-3 cells, however sparing the normal cells. Thus it can be concluded that the silver nanoparticles of *Tabebuia pallida* loaded liposomes achieve targeted delivery at tumor site thereby minimize the adverse effects caused during cancer therapy as the liposomes are non-toxic to normal PBL.